

# On $O(\max\{n_1, n_2\} \log(\max\{n_1, n_2\}n_3))$ Sample Entries for $n_1 \times n_2 \times n_3$ Tensor Completion via Unitary Transformation\*

Guang-Jing Song<sup>†</sup>      Michael K. Ng<sup>‡</sup>      Xiongjun Zhang<sup>§</sup>

December 22, 2024

**Abstract:** One of the key problems in tensor completion is the number of uniformly random sample entries required for recovery guarantee. The main aim of this paper is to study  $n_1 \times n_2 \times n_3$  third-order tensor completion and investigate into incoherence conditions of  $n_3$  low-rank  $n_1$ -by- $n_2$  matrix slices under the transformed tensor singular value decomposition where the unitary transformation is applied along  $n_3$ -dimension. We show that such low-rank tensors can be recovered exactly with high probability when the number of randomly observed entries is of order  $O(r \max\{n_1, n_2\} \log(\max\{n_1, n_2\}n_3))$ , where  $r$  is the sum of the ranks of these  $n_3$  matrix slices in the transformed tensor. By utilizing synthetic data and imaging data sets, we demonstrate that the theoretical result can be obtained under valid incoherence conditions, and the tensor completion performance of the proposed method is also better than that of existing methods in terms of sample sizes requirement.

**Keywords:** tensor completion, transform tensor singular value decomposition, sampling sizes, transformed tubal nuclear norm

**AMS Subject Classifications 2010:** 15A69, 15A83, 90C25

## 1 Introduction

The problem of recovering an unknown low-rank tensor from a small fraction of its entries is known as the tensor completion problem, and comes up in a wide range of applications, e.g., [11, 23, 33], computer vision [18, 36], and machine learning [26, 27]. The goal of low-rank tensor completion is to recover a tensor with the lowest rank based on observable entries of a given tensor  $\mathcal{M} \in \mathbb{C}^{n_1 \times n_2 \times n_3}$  indexed by  $\Omega$ , which can be expressed as follows:

$$\begin{aligned} \min_{\mathcal{Z}} \quad & \text{rank}(\mathcal{Z}) \\ \text{s.t.} \quad & \mathcal{P}_{\Omega}(\mathcal{Z}) = \mathcal{P}_{\Omega}(\mathcal{M}), \end{aligned} \tag{1}$$

\*The research of M. K. Ng was supported in part by the HKRGC GRF 12306616, 12200317, 12300218 and 12300519. The research of X. Zhang was supported in part by the National Natural Science Foundation of China under grants 11801206, 11871025, Hubei Provincial Natural Science Foundation of China under grant 2018CFB105, and Fundamental Research Funds for the Central Universities under grant CCNU19ZN017.

<sup>†</sup>G.-J. Song is with the School of Mathematics and Information Sciences, Weifang University, Weifang 261061, China (e-mail: sgjshu@163.com).

<sup>‡</sup>M. Ng is with the Department of Mathematics, The University of Hong Kong, Hong Kong (e-mail: mng@maths.hku.hk).

<sup>§</sup>X. Zhang is with the School of Mathematics and Statistics and Hubei Key Laboratory of Mathematical Sciences, Central China Normal University, Wuhan 430079, China (e-mail: xjzhang@mail.ccnu.edu.cn).

where  $\Omega$  is a subset of  $\{1, \dots, n_1\} \times \{1, \dots, n_2\} \times \{1, \dots, n_3\}$  and  $\mathcal{P}_\Omega$  is the projection operator such that the entries in  $\Omega$  are given while the remaining entries are missing, i.e.,

$$(\mathcal{P}_\Omega(\mathcal{Z}))_{ijk} = \begin{cases} \mathcal{Z}_{ijk}, & \text{if } (i, j, k) \in \Omega, \\ 0, & \text{otherwise.} \end{cases}$$

In particular, if  $n_3 = 0$ , the tensor completion problem (1) reduces to the well-known matrix completion problem, which has received a considerable amount of attention in the past decades, see, e.g., [3, 4, 5, 9, 25] and references therein. In matrix completion case, a given incoherent  $n \times n$  matrix could be recovered with high probability if the uniformly random sample size is of order  $O(rn \log n)$ , where  $r$  is the rank of the given matrix. This bound has been shown to be optimal, see [5] for detailed discussions.

The main aim of this paper is to study incoherence conditions of low-rank tensors under transformed tensor singular value decomposition and provide a lower bound on the number of random sample entries required for exact tensor recovery. Different kinds of tensor rank lead to different convex relaxation models and different sample sizes required for exact recovery. When the rank in the model (1) is chosen as the Tucker rank [30], Liu et al. [18] proposed to use the sum of the nuclear norms (SNN) of unfolding matrices of a tensor to recover a low Tucker rank tensor. Under the SNN framework, Tomioka et al. [29] proved that a given  $m$ th-order tensor  $\mathcal{X} \in \mathbb{R}^{n \times n \times \dots \times n}$  with Tucker rank  $(r, r, \dots, r)$  can be exactly recovered with high probability if the Gaussian measurements size is of order  $O(rn^{m-1})$ . Later, Mu et al. [21] proved that  $O(rn^{m-1})$  Gaussian measurements are necessary for a reliable recovery under the SNN framework. In fact, the degrees of freedom of a tensor  $\mathcal{X} \in \mathbb{R}^{n \times n \times \dots \times n}$  with Tucker rank  $(r_1, r_2, \dots, r_m)$  are  $\prod_{i=1}^m r_i + \sum_{i=1}^m (r_i n - r_i^2)$ , which is much smaller than  $O(rn^{m-1})$ . This implies that there exists room for improvement for tensor completion. Recently, Yuan et al. [34, 35] showed that an  $n \times n \times n$  tensor with Tucker rank  $(r, r, r)$  can be recovered exactly with high probability with as few as  $O((r^{\frac{1}{2}} n^{\frac{3}{2}} + r^2 n) \log^2(n))$  entries observed. These sample size requirement drastically improves those based on unfolding methods which typically require a sample size of the order given in [21]. Later, Xia et al. [32] showed that an  $n \times n \times n$  tensor with multilinear rank  $(r, r, r)$  can be reconstructed with high probability from as few as  $O(r^{\frac{7}{2}} n^{\frac{3}{2}} \log^{\frac{3}{2}} n + r^7 n \log^6 n)$  entries by a gradient descent algorithm. When the rank in the model (1) is chosen as the CANDECOMP/PARAFAC (CP) rank [16], Mu et al. [21] introduced a square deal method which only uses an individual nuclear norm of a balanced matrix instead of using a combination of all  $m$  nuclear norms of unfolding matrices of the tensor. Under this setting, they also proved that  $O(r^{\lfloor \frac{m}{2} \rfloor} n^{\lceil \frac{m}{2} \rceil})$  samples are sufficient to recover a CP rank  $r$  tensor with high probability.

The tubal rank of a third-order tensor is proposed by Kilmer et al. [14, 15]. The tubal rank is based on tensor-tensor product (t-product) and the associated algebraic framework allows tensor factorizations like matrix factorizations. This new perspective has endowed multidimensional data arrays with an advantageous representation in real-world applications. Zhang et al. [37] used the tensor tubal nuclear norm (TNN) as a convex relaxation of the tensor tubal rank, and then proved that a low tubal rank tensor can be exactly recovered by  $O(rn^2 \log(n^2))$  uniformly sampled entries. However, the TNN is not the convex envelope of the tubal rank which may lead to more sample entries needed to exactly recover the original tensor. In Table 1, we summarize existing tensor completion results for  $n \times n \times n$  third-order tensors. It is interesting to note that there are other factors that affect sample sizes required, e.g., sampling methods and incoherence conditions. For detailed discussions, we refer to the references [1, 12, 17, 20].

In this paper, we mainly study tensor completion for third-order tensors of size  $n_1 \times n_2 \times n_3$  and investigate into incoherence conditions of  $n_3$  low-rank matrix slices of sizes  $n_1 \times n_2$  under

Table 1: A summary of sample sizes and sampling methods for tensor completion.

| Rank Assumption                                | Sampling Method  | Incoherent and Other Conditions                     | Requirement Sampling Sizes   |
|--|------------------|---|--|
| CP-rank $r$ [21]                               | Gaussian         | N/A   | $O(rn^2)$  |
| CP-rank $r$ [12]                               | Uniformly Random | Incoherent condition of symmetric tensor            | $O(n^{\frac{3}{2}}r^5\log^4(n))$                                     |
| Tucker rank [35]<br>( $r, r, r$ )              | Uniformly Random | Matrix incoherent condition on model- $n$ unfolding | $O(rn^{\frac{3}{2}} + r^2n)\log^2(n)$                                |
| Tucker rank [10]<br>( $r, r, r$ )              | Random           | Matrix incoherent condition on model- $n$ unfolding | $O(rn^2\log^2(n))$   |
| Tucker rank [21]<br>( $r, r, r$ )              | Gaussian         | N/A   | $O(rn^2)$  |
| Tucker rank [32]<br>( $r, r, r$ )              | Uniformly Random | Matrix incoherent condition on model- $n$ unfolding | $O(r^{\frac{7}{2}}n^{\frac{3}{2}}\log^{\frac{3}{2}}n + r^7n\log^6n)$ |
| Tubal rank $r$ [37]                            | Uniformly Random | Tensor incoherent condition                         | $O(rn^2\log(n^2))$   |
| multi-rank ( $r_1, r_2, r_3$ )<br>(this paper) | Uniformly Random | Tensor incoherent condition                         | $O(\sum r_i n \log(n^2))$  |

the transformed tensor singular value decomposition. We show that such low-rank tensors can be recovered exactly with high probability when the number of randomly observed entries is of order  $O(r \max\{n_1, n_2\} \log(\max\{n_1, n_2\}n_3))$ , where  $r$  is the sum of the ranks of these  $n_3$  matrix slices in the transformed tensor.

The outline of this paper is given as follows. In Section 2, the transformed tensor singular value decomposition by using unitary transformation is reviewed. In Section 3, we provide the bound on the number of sample entries for tensor completion via unitary transformation. In Section 4, several synthetic data and imaging data sets by using different transformations are performed to demonstrate that our theoretical result is valid and the performance of the proposed method is better than that of existing methods in terms of sample sizes requirement. Finally, some concluding remarks are given in Section 5.

## 2 Transformed Tensor Singular Value Decomposition

Before continuing, let us survey some notation and definitions used throughout this paper. We denote  $\Phi$  as an arbitrary unitary matrix, i.e.,  $\Phi\Phi^H = \Phi^H\Phi = I$ , where  $\Phi^H$  denotes the conjugate transpose of  $\Phi$  and  $I$  is an identity matrix whose dimension should be clear from the context. For any third-order tensor  $\mathcal{A} \in \mathbb{C}^{n_1 \times n_2 \times n_3}$ ,  $\hat{\mathcal{A}}_\Phi$  denotes a third-order tensor obtained as follows:

$$\text{vec}(\hat{\mathcal{A}}_\Phi(i, j, :)) = \Phi(\text{vec}(\mathcal{A}(i, j, :))),$$

where  $\text{vec}(\cdot)$  is the vectorization operator from  $\mathbb{C}^{1 \times 1 \times n_3}$  to  $\mathbb{C}^{n_3}$ . For simplicity, we denote  $\hat{\mathcal{A}}_\Phi = \Phi[\mathcal{A}]$ . In the same fashion, one can also compute  $\mathcal{A}$  from  $\hat{\mathcal{A}}_\Phi$ , i.e.,  $\mathcal{A} = \Phi^H[\hat{\mathcal{A}}_\Phi]$ . A

block diagonal matrix can be derived by the frontal slices of  $\mathcal{A}$  by the “blockdiag” operator:

$$\overline{\mathcal{A}} = \text{blockdiag}(\mathcal{A}) := \begin{pmatrix} \mathcal{A}^{(1)} & & & \\ & \mathcal{A}^{(2)} & & \\ & & \ddots & \\ & & & \mathcal{A}^{(n_3)} \end{pmatrix},$$

where  $\mathcal{A}^{(i)}$  is the  $i$ -th frontal slices of  $\mathcal{A}$ ,  $i = 1, \dots, n_3$ . Conversely, the block diagonal matrix  $\overline{\mathcal{A}}$  can be converted into a tensor via the following “fold” operator:

$$\text{fold}(\text{blockdiag}(\mathcal{A})) := \mathcal{A}.$$

After introducing the tensor notation and terminology, we give the basic definitions on the tensor product, the conjugate transpose of a tensor, the identity tensor and the unitary tensor with respect to the unitary transformation matrix  $\Phi$ , respectively.

**Definition 2.1.** The  $\Phi$ -product of  $\mathcal{A} \in \mathbb{C}^{n_1 \times n_2 \times n_3}$  and  $\mathcal{B} \in \mathbb{C}^{n_2 \times n_4 \times n_3}$  is a tensor  $\mathcal{C} \in \mathbb{C}^{n_1 \times n_4 \times n_3}$ , which is given by

$$\mathcal{C} = \mathcal{A} \diamond_{\Phi} \mathcal{B} = \Phi^H \left[ \text{fold} \left( \text{blockdiag}(\hat{\mathcal{A}}_{\Phi}) \cdot \text{blockdiag}(\hat{\mathcal{B}}_{\Phi}) \right) \right].$$

**Remark 2.1.** Kernfeld et al. [13] defined the tensor product between two tensors by using the slices products in the transformed field based on any arbitrary invertible transformation. In this paper, we mainly focus on the tensor product based on unitary transformations. Moreover, the relation between  $\Phi$ -product and tensor product by using fast Fourier transform [15] is shown in [28].

**Definition 2.2.** For any  $\mathcal{A} \in \mathbb{C}^{n_1 \times n_2 \times n_3}$ , its conjugate transpose with respect to  $\Phi$ , denoted by  $\mathcal{A}^H \in \mathbb{C}^{n_2 \times n_1 \times n_3}$ , is defined as

$$\mathcal{A}^H = \Phi^H \left[ \text{fold} \left( \text{blockdiag}(\hat{\mathcal{A}}_{\Phi})^H \right) \right].$$

**Definition 2.3.** [13, Proposition 4.1] The identity tensor  $\mathcal{I}_{\Phi} \in \mathbb{C}^{n \times n \times n_3}$  (with respect to  $\Phi$ ) is defined to be a tensor such that  $\mathcal{I}_{\Phi} = \Phi^H[\mathcal{T}]$ , where  $\mathcal{T} \in \mathbb{C}^{n \times n \times n_3}$  with each frontal slice being the  $n \times n$  identity matrix.

**Definition 2.4.** [13, Definition 5.1] A tensor  $\mathcal{Q} \in \mathbb{C}^{n \times n \times n_3}$  is unitary with respect to  $\Phi$ -product if it satisfies

$$\mathcal{Q}^H \diamond_{\Phi} \mathcal{Q} = \mathcal{Q} \diamond_{\Phi} \mathcal{Q}^H = \mathcal{I}_{\Phi}.$$

In addition,  $\mathcal{A}$  is a diagonal tensor if and only if each frontal slice  $\mathcal{A}^{(i)}$  is a diagonal matrix. The transformed tensor singular value decomposition (SVD) with respect to  $\Phi$  can be given as follows.

**Theorem 2.2.** [13, Theorem 5.1] Suppose that  $\mathcal{A} \in \mathbb{C}^{n_1 \times n_2 \times n_3}$ . Then  $\mathcal{A}$  can be factorized as

$$\mathcal{A} = \mathcal{U} \diamond_{\Phi} \mathcal{S} \diamond_{\Phi} \mathcal{V}^H, \quad (2)$$

where  $\mathcal{U} \in \mathbb{C}^{n_1 \times n_1 \times n_3}$ ,  $\mathcal{V} \in \mathbb{C}^{n_2 \times n_2 \times n_3}$  are unitary tensors with respect to  $\Phi$ -product, and  $\mathcal{S} \in \mathbb{C}^{n_1 \times n_2 \times n_3}$  is a diagonal tensor.

Based on the transformed tensor SVD given in Theorem 2.2, the transformed multi-rank and tubal rank of a tensor can be defined as follows.

**Definition 2.5.** The transformed multi-rank of  $\mathcal{A} \in \mathbb{C}^{n_1 \times n_2 \times n_3}$  denoted as  $\text{rank}_t(\mathcal{A})$ , is a vector  $\mathbf{r} \in \mathbb{R}^{n_3}$  with its  $i$ -th entry as the rank of the  $i$ -th frontal slice of  $\hat{\mathcal{A}}$ , i.e.,

$$\text{rank}_t(\mathcal{A}_\Phi) = \mathbf{r}, \quad r_i = \text{rank}(\hat{\mathcal{A}}_\Phi^{(i)}), \quad i = 1, \dots, n_3.$$

The transformed tubal rank of  $\mathcal{A} \in \mathbb{C}^{n_1 \times n_2 \times n_3}$ , denoted as  $\text{rank}_{tt}(\mathcal{A})$ , is defined as the number of nonzero singular tubes of  $\mathcal{S}$ , where  $\mathcal{S}$  comes from the transformed  $t$ -SVD of  $\mathcal{A}$ , i.e.,

$$\text{rank}_{tt}(\mathcal{A}) = \#\{i : \mathcal{S}(i, i, :) \neq \mathbf{0}\} = \max_i r_i. \quad (3)$$

**Remark 2.3.** For computational improvement, we will use the skinny transformed tensor SVD throughout the paper unless otherwise stated, which is defined as follows: The skinny transformed tensor SVD of  $\mathcal{A} \in \mathbb{C}^{n_1 \times n_2 \times n_3}$  with  $\text{rank}_{tt}(\mathcal{A}) = r$  is given as  $\mathcal{A} = \mathcal{U} \diamond_\Phi \mathcal{S} \diamond_\Phi \mathcal{V}^H$ , where  $\mathcal{U} \in \mathbb{C}^{n_1 \times r \times n_3}$  and  $\mathcal{V} \in \mathbb{C}^{n_2 \times r \times n_3}$  satisfying  $\mathcal{U}^H \diamond_\Phi \mathcal{U} = \mathcal{I}_r$ ,  $\mathcal{V}^H \diamond_\Phi \mathcal{V} = \mathcal{I}_r$  and  $\mathcal{S} \in \mathbb{C}^{r \times r \times n_3}$  is a diagonal tensor.

The following fact will be used throughout the paper. For any tensor  $\mathcal{A} \in \mathbb{C}^{n_1 \times n_2 \times n_3}$  and  $\mathcal{B} \in \mathbb{C}^{n_2 \times n_4 \times n_3}$ , we have  $\mathcal{A} \diamond_\Phi \mathcal{B} = \mathcal{C} \Leftrightarrow \bar{\mathcal{A}}_\Phi \cdot \bar{\mathcal{B}}_\Phi = \bar{\mathcal{C}}_\Phi$ . The inner product of two tensors  $\mathcal{A}, \mathcal{B} \in \mathbb{C}^{n_1 \times n_2 \times n_3}$  can be defined as

$$\langle \mathcal{A}, \mathcal{B} \rangle = \sum_{i=1}^{n_3} \langle \mathcal{A}^{(i)}, \mathcal{B}^{(i)} \rangle = \langle \bar{\mathcal{A}}_\Phi, \bar{\mathcal{B}}_\Phi \rangle, \quad (4)$$

where  $\langle \mathcal{A}^{(i)}, \mathcal{B}^{(i)} \rangle$  is the usual inner product of two matrices.

For any  $\mathcal{A} \in \mathbb{C}^{n_1 \times n_2 \times n_3}$ , the tensor spectral norm of  $\mathcal{A}$  relate to  $\Phi$ , denoted as  $\|\mathcal{A}\|$ , can be defined as  $\|\mathcal{A}\| = \|\bar{\mathcal{A}}_\Phi\|$  [28], i.e., the spectral norm of its block diagonal matrix in the transformed domain. Suppose that  $\mathcal{L}$  is a tensor operator, its operator norm is defined as  $\|\mathcal{L}\|_{\text{op}} = \sup_{\|\mathcal{A}\|_F \leq 1} \|\mathcal{L}(\mathcal{A})\|_F$ . If it can be represented as a tensor  $\mathcal{L}$  via  $\Phi$ -product with  $\mathcal{A}$ , we have  $\|\mathcal{L}\|_{\text{op}} = \|\mathcal{L}\|$ . Moreover, the tensor infinity norm, the tensor Frobenius norm, the tensor  $l_{\infty,2}$  and the tensor weighted  $l_{\infty,w}$  norm are respectively defined as

$$\begin{aligned} \|\mathcal{A}\|_\infty &= \max_{ijk} |\mathcal{A}_{ijk}|, \quad \|\mathcal{A}\|_F = \sqrt{\sum_{ijk} |\mathcal{A}_{ijk}|^2}, \\ \|\mathcal{A}\|_{\infty,2} &= \max \left\{ \max_i \sqrt{\sum_{b,k} \mathcal{A}_{ibk}^2}, \max_j \sqrt{\sum_{a,k} \mathcal{A}_{ajk}^2} \right\}, \end{aligned}$$

and

$$\|\mathcal{A}\|_{\infty,w} = \max \left\{ \max_i \sqrt{\sum_{b,k} \alpha_k^2 \mathcal{A}_{ibk}^2}, \max_j \sqrt{\sum_{a,k} \beta_k^2 \mathcal{A}_{ajk}^2} \right\}, \quad (5)$$

where  $\sum_{k=1}^{n_3} \alpha_k^2 = \sum_{k=1}^{n_3} \beta_k^2 = 1$ . The aim of this paper is to recover a low transformed multi-rank tensor, which motivates us to introduce the following definition of tensor nuclear norm.

**Definition 2.6.** The transformed tubal nuclear norm of a tensor  $\mathcal{A} \in \mathbb{C}^{n_1 \times n_2 \times n_3}$ , denoted as  $\|\mathcal{A}\|_{\text{TTNN}}$ , is the sum of the nuclear norms of all the frontal slices of  $\hat{\mathcal{A}}_\Phi$ , i.e.,  $\|\mathcal{A}\|_{\text{TTNN}} = \sum_{i=1}^{n_3} \|\hat{\mathcal{A}}_\Phi^{(i)}\|_*$ .

Recently, Song et al. [28] showed that the transformed tubal nuclear norm (TTNN) of a tensor is the convex envelope of the sum of the entries of the transformed multi-rank of a tensor, which can be stated in the following.

**Lemma 2.4.** [28, Lemma 1] For any tensor  $\mathcal{X} \in \mathbb{C}^{n_1 \times n_2 \times n_3}$ ,  $\text{rank}_{\text{sum}}(\mathcal{X}) = \sum_{i=1}^{n_3} \text{rank}(\hat{\mathcal{X}}_{\Phi}^{(i)})$  denotes a transformed multi-rank function. Then  $\|\mathcal{X}\|_{\text{TTNN}}$  is the convex envelope of the function  $\text{rank}_{\text{sum}}(\mathcal{X})$  on the set  $\{\mathcal{X} \mid \|\mathcal{X}\| \leq 1\}$ .

Lemma 2.4 shows that the TTNN is the convex envelope of the transformed multi-rank tensor over a unit ball of the tensor spectral norm. That is why the TTNN is effective in studying the tensor recovery theory with multi-rank minimization. Next, we introduce two kinds of tensor basis which will be exploited to derive our main results.

**Definition 2.7.** (i) The transformed column basis with respect to  $\Phi$ , where  $\Phi^* \Phi = I$ , denoted as  $\vec{e}_{ik}$ , is a tensor of size  $n_1 \times 1 \times n_3$  with the  $(i, 1, k)$ -th element equaling to 1 and the others equaling to 0. (ii) Denote  $\hat{e}_k$  as a tensor of size  $1 \times 1 \times n_3$  with the  $(1, 1, k)$ -th entry equaling to 1 and the remaining entries equaling to 0,  $\Phi(\hat{e}_k)_t$  as the  $(1, 1, t)$ -th entry of  $\Phi(\hat{e}_k)$ ,  $t = 1, \dots, n_3$ . The transformed tube basis with respect to  $\Phi$ , denoted as  $\hat{e}_{kt}$ , is a tensor of size  $1 \times 1 \times n_3$  with the  $(1, 1, t)$ -th entry of  $\Phi(\hat{e}_{kt})$  equaling to  $(\Phi(\hat{e}_k)_t)^{-1}$ , if  $\Phi(\hat{e}_k)_t \neq 0$ , and 0, otherwise.

### 3 Main Results

In this section, we consider the tensor completion problem, which aims to recover a low transformed multi-rank tensor under some limited observations. Mathematically, the problem can be described as follows:

$$\begin{aligned} \min_{\mathcal{Z}} \quad & \text{rank}_t(\mathcal{Z}) \\ \text{s.t.} \quad & \mathcal{P}_{\Omega}(\mathcal{Z}) = \mathcal{P}_{\Omega}(\mathcal{M}), \end{aligned}$$

where  $\text{rank}_t(\mathcal{Z})$  is the transformed multi-rank,  $\Omega$  and  $\mathcal{P}_{\Omega}(\mathcal{Z})$  are given as in model (1). In general, which is similar to the matrix case, a convex relaxation is proposed by using transformed tensor nuclear norm. More precisely speaking, the convex relaxation model is given by

$$\begin{aligned} \min_{\mathcal{Z}} \quad & \|\mathcal{Z}\|_{\text{TTNN}} \\ \text{s.t.} \quad & \mathcal{P}_{\Omega}(\mathcal{Z}) = \mathcal{P}_{\Omega}(\mathcal{M}). \end{aligned} \tag{6}$$

As discussed in matrix completion problems, exact recovery is hopeless if most entries are equal to zero. To make the problem meaningful, we first need some incoherence conditions on tensor to ensure that it is not sparse.

**Definition 3.1.** Let  $\mathcal{Z} \in \mathbb{C}^{n_1 \times n_2 \times n_3}$  with  $\text{rank}_t(\mathcal{Z}) = \mathbf{r}$ . Assume its skinny transformed tensor SVD is  $\mathcal{Z} = \mathcal{U} \diamond_{\Phi} \mathcal{S} \diamond_{\Phi} \mathcal{V}^H$ . Then  $\mathcal{Z}$  is said to satisfy the tensor incoherence conditions, if there exist a parameter  $\mu \geq 1$ , such that

$$\max_{i=1, \dots, n_1} \max_{k=1, \dots, n_3} \|\mathcal{U}^H \diamond_{\Phi} \vec{e}_{ik}\|_F \leq \sqrt{\frac{\mu \sum_{i=1}^{n_3} r_i}{n_1 n_3}}, \tag{7}$$

$$\max_{j=1, \dots, n_2} \max_{k=1, \dots, n_3} \|\mathcal{V}^H \diamond_{\Phi} \vec{e}_{jk}\|_F \leq \sqrt{\frac{\mu \sum_{i=1}^{n_3} r_i}{n_2 n_3}}, \tag{8}$$

where  $\vec{e}_{ik}$  and  $\vec{e}_{jk}$  are the tensor basis with respect to the transformation  $\Phi$ .

Denote by  $T$  the linear space of tensors

$$T = \{\mathcal{U} \diamond_{\Phi} \mathcal{Y}^H + \mathcal{W} \diamond_{\Phi} \mathcal{V}^H \mid \mathcal{Y} \in \mathbb{C}^{n_2 \times r \times n_3}, \mathcal{W} \in \mathbb{C}^{n_1 \times r \times n_3}\}, \quad (9)$$

and by  $T^\perp$  its orthogonal complement, where  $\mathcal{U} \in \mathbb{C}^{n_1 \times r \times n_3}$  and  $\mathcal{V} \in \mathbb{C}^{n_2 \times r \times n_3}$  are column unitary tensors, respectively. In the light of [36, Proposition B.1], for any  $\mathcal{Z} \in \mathbb{C}^{n_1 \times n_2 \times n_3}$ , the orthogonal projections onto  $T$  and its complementary are given as follows:

$$\begin{aligned} \mathcal{P}_T(\mathcal{Z}) &= \mathcal{U} \diamond_{\Phi} \mathcal{U}^H \diamond_{\Phi} \mathcal{Z} + \mathcal{Z} \diamond_{\Phi} \mathcal{V} \diamond_{\Phi} \mathcal{V}^H - \mathcal{U} \diamond_{\Phi} \mathcal{U}^H \diamond_{\Phi} \mathcal{Z} \diamond_{\Phi} \mathcal{V} \diamond_{\Phi} \mathcal{V}^H, \\ \mathcal{P}_{T^\perp}(\mathcal{Z}) &= (\mathcal{I}_{\Phi} - \mathcal{U} \diamond_{\Phi} \mathcal{U}^H) \diamond_{\Phi} \mathcal{Z} \diamond_{\Phi} (\mathcal{I}_{\Phi} - \mathcal{V} \diamond_{\Phi} \mathcal{V}^H). \end{aligned}$$

Denote  $n_{(1)} = \max\{n_1, n_2\}$ ,  $n_{(2)} = \min\{n_1, n_2\}$ , and then we improve the low bound of the sampling sizes for tensor completion in the following theorem.

**Theorem 3.1.** *Suppose that  $\mathcal{Z} \in \mathbb{C}^{n_1 \times n_2 \times n_3}$  with  $\text{rank}_t(\mathcal{Z}) = \mathbf{r}$  and its skinny transformed tensor SVD is  $\mathcal{Z} = \mathcal{U} \diamond_{\Phi} \mathcal{S} \diamond_{\Phi} \mathcal{V}^H$ , where  $\mathcal{U} \in \mathbb{C}^{n_1 \times r \times n_3}$ ,  $\mathcal{S} \in \mathbb{C}^{r \times r \times n_3}$  and  $\mathcal{V} \in \mathbb{C}^{n_2 \times r \times n_3}$ . Suppose that  $\mathcal{Z}$  satisfies the incoherence conditions (7)-(8) and the observation set  $\Omega$  with  $|\Omega| = m$  is uniformly distributed among all sets of cardinality, then there exist universal constants  $c_0, c_1, c_2 > 0$  such that if*

$$m \geq c_0 \mu \sum_{i=1}^{n_3} r_i n_{(1)} \log(n_{(1)} n_3), \quad (10)$$

$\mathcal{Z}$  is the unique minimizer to (6) with probability at least  $1 - c_1(n_{(1)} n_3)^{-c_2}$ .

Theorem 3.1 greatly improves prior results in [37]. First of all, it reduces the sampling sizes needed to exactly recover a low rank tensor with weaker assumptions. Second, it shows that the exact recovery theory not only holds for the fast Fourier transform (FFT) but also for any unitary transformation, which is very meaningful in practical applications. Based on the new results, for the given data, we can choose an optimal unitary transformation such that the tensor possess a low rank property in the transform domain, which guarantees to derive better results than that by using the FFT directly.

To facilitate our proof of the main theorem, we will consider the independent and identical distribution (*i.i.d.*) *Bernoulli-Rademacher model*. More precisely, we assume  $\Omega = \{(i, j, k) \mid \delta_{ijk} = 1\}$ , where  $\delta_{ijk}$  are i.i.d. Bernoulli variables taking value one with probability  $\rho$  and zero with probability  $1 - \rho$ . Such a Bernoulli sampling is denoted by  $\Omega \sim \text{Ber}(\rho)$  for short. As a proxy for uniform sampling, the probability of failure under Bernoulli sampling with  $\rho = \frac{m}{n_1 n_2 n_3}$  closely approximates the probability of failure under uniform sampling.

Before moving on, we need to pay attention to the following conclusions which play important roles in proving Lemmas 3.3, 3.4 and 3.5, respectively. Recall the definition of tensor Frobenius norm and the transformed tensor incoherence conditions given in (7)-(8), we can get the result easily. So we omit the proof process and only list the conclusion.

**Proposition 3.2.** *Let  $\mathcal{Z} \in \mathbb{C}^{n_1 \times n_2 \times n_3}$  be an arbitrary tensor, and  $T$  be given as (9). Suppose that the transformed tensor incoherence conditions (7)-(8) are satisfied, then*

$$\|\mathcal{P}_T(\vec{e}_{ik} \diamond_{\Phi} \vec{e}_{kt} \diamond_{\Phi} \vec{e}_{jk}^H)\|_F^2 \leq \frac{2\mu \sum_{i=1}^{n_3} r_i}{n_{(2)} n_3}.$$

Next, we list several key lemmas which play crucial roles in the proof of the main result.

**Lemma 3.3.** Suppose that  $\Omega \sim \text{Ber}(\rho)$ , where  $\Omega$  with  $|\Omega| = m$  is a set of indices sampled independently and uniformly without replacement,  $\rho = \frac{m}{n_1 n_2 n_3}$  and  $T$  is given as (9). Then with high probability,

$$\|\rho^{-1} \mathcal{P}_T \mathcal{P}_\Omega \mathcal{P}_T - \mathcal{P}_T\|_{op} \leq \epsilon, \quad (11)$$

provided that  $m \geq C_0 \epsilon^{-2} \mu \sum r_i n_1 \log(n_{(1)} n_3)$  for some numerical constant  $C_0 > 0$ .

**Lemma 3.4.** Suppose that  $\mathcal{Z} \in \mathbb{C}^{n_1 \times n_2 \times n_3}$  is a fixed tensor,  $\Omega, \rho$  and  $m$  are defined as Lemma 3.3. Then for all  $c, \beta > 1$ , and  $C_0 > 0$

$$\|(\rho^{-1} \mathcal{P}_\Omega - \mathcal{I})\mathcal{Z}\| \leq c \left( \frac{\log n_{(1)} n_3}{\rho} \|\mathcal{Z}\|_\infty + \sqrt{\frac{\log n_{(1)} n_3}{\rho}} \|\mathcal{Z}\|_{\infty, w} \right)$$

holds with high probability provided that  $m \geq C_0 \epsilon^{-2} \mu \sum_{i=1}^{n_3} r_i n_{(1)} \log(n_{(1)} n_3)$ .

**Lemma 3.5.** Suppose that  $\mathcal{Z} \in \mathbb{C}^{n_1 \times n_2 \times n_3}$  is a fixed tensor,  $\Omega, \rho$  and  $m$  are defined as Lemma 3.3. Then for some sufficiently large  $c_0$

$$\|(\rho^{-1} \mathcal{P}_T \mathcal{P}_\Omega - \mathcal{P}_T)\mathcal{Z}\|_{\infty, w} \leq \frac{1}{2} \sqrt{\frac{n_1 n_3}{\mu \sum_{i=1}^{n_3} r_i}} \|\mathcal{Z}\|_\infty + \frac{1}{2} \|\mathcal{Z}\|_{\infty, w} \quad (12)$$

holds with high probability provided that  $m \geq C_0 \epsilon^{-2} \mu \sum_{i=1}^{n_3} r_i n_{(1)} \log(n_{(1)} n_3)$ .

Lemma 3.4 gives the bound of the spectral norm of  $(\rho^{-1} \mathcal{P}_\Omega - \mathcal{I})\mathcal{Z}$  in terms of  $\|\mathcal{Z}\|_\infty$  and  $\|\mathcal{Z}\|_{\infty, w}$ , which is tighter than the previous approaches that use the  $\|\mathcal{Z}\|_\infty$  and  $\|\mathcal{Z}\|_{\infty, 2}$ . Moreover, the weights in  $\|\mathcal{Z}\|_{\infty, w}$  are determined by the unitary transformation, which guarantee this upper bound is tightest. Lemma 3.5 can further control the  $\|\mathcal{Z}\|_{\infty, w}$  norm. We will prove them in the Appendix. Moreover, Lemmas C1 and C2 in [37] can be seen as special cases of Lemmas 3.4 and 3.5, respectively, if the transformation is chosen as FFT, and the tensors are studied over the real number field.

**Lemma 3.6** (Lemma 4.1 in [37]). Suppose that  $\|\rho^{-1} \mathcal{P}_T \mathcal{P}_\Omega \mathcal{P}_T - \mathcal{P}_T\|_{op} \leq \frac{1}{2}$ . Then for any  $\mathcal{Z}$  such that  $\mathcal{P}_\Omega(\mathcal{Z}) = 0$ , we have

$$\frac{1}{2} \|\mathcal{P}_{T^\perp}(\mathcal{Z})\|_{\text{TTNN}} > \frac{1}{4n_{(1)} n_3} \|\mathcal{P}_T(\mathcal{Z})\|_F$$

with high probability.

With the tools in hand we can list the proof of Theorem 3.1 in details.

**Proof of Theorem 3.1.** The high level road map of the proof is a standard one just as shown in Candès et al. [2]: by convex analysis, to show  $\mathcal{M}$  is the unique optimal solution to the problem (6), it is sufficient to find a dual certificate  $\mathcal{Y}$  satisfying several subgradient type conditions. In our case, we need to find a tensor  $\mathcal{Y} = \mathcal{P}_\Omega(\mathcal{Y})$  such that

$$\|\mathcal{P}_T(\mathcal{Y}) - \mathcal{U} \diamond_{\Phi} \mathcal{V}^H\|_F \leq \frac{1}{4n_{(1)} n_3^2}, \quad (13)$$

$$\|\mathcal{P}_{T^\perp}(\mathcal{Y})\| \leq \frac{1}{2}. \quad (14)$$

It follows from (14) that the spectral norm of  $\|\mathcal{P}_{T^\perp}(\mathcal{Y})\|$  need to be small. There are some other kinds of tensor norm can be chosen to bound the spectral norm. For example



in [2],  $\|\mathcal{Y}\|_\infty$  is used to bound  $\|\mathcal{Y}\|$  which ultimately links to  $\|\mathcal{U} \diamond_{\Phi} \mathcal{V}^H\|_\infty$  and leads to the joint incoherence condition similar to the matrix case. In order to avoid applying the joint incoherence condition,  $\|\mathcal{Y}\|_{\infty,2}$  is used in [6] and [37], to bound  $\|\mathcal{Y}\|$  for matrix and tensor case, respectively. Then a tighter bound is derived. However, for arbitrary unitary transformation, the bound derived by  $\|\mathcal{Y}\|_{\infty,2}$  is relaxed again. Here, we derive a new bound using the  $l_{\infty,w}$  norm  $\|\mathcal{Y}\|_{\infty,w}$  as defined in (5). Note that  $\|\mathcal{Y}\|_{\infty,w}$  is not greater than  $\|\mathcal{Y}\|_{\infty,2}$  for any tensor  $\mathcal{Y}$ , which leads to a tighter bound of  $\|\mathcal{Y}\|$ .

We now turn to the proof in details. We apply the Golfing Scheme method introduced by Gross [9] and modified by Candès et al. [2] to construct a dual tensor  $\mathcal{Y}$  supported by  $\Omega$  iteratively. Similar to the proof of [37, Theorem 3.1], we consider the set  $\Omega \sim \text{Ber}(\rho)$  as a union of sets of support  $\Omega_j$ , i.e.,  $\Omega = \bigcup_{j=1}^p \Omega_j$ , where  $\Omega_j \sim \text{Ber}(q)$ , which implies  $q \geq C_0 \rho / \log(n_{(1)} n_3)$ . Hence we have  $1 - \rho = (1 - q)^p$ , where  $p = \lceil 5 \log(n_{(1)} n_3) + 1 \rceil$ . Denote

$$\mathcal{Y} = \sum_{j=1}^p \frac{1}{q_j} \mathcal{P}_{\Omega_j}(\mathcal{Z}_{j-1}), \text{ with } \mathcal{Z}_j = \left( \mathcal{P}_T - \frac{1}{q_j} \mathcal{P}_T \mathcal{P}_{\Omega_j} \mathcal{P}_T \right) \mathcal{Z}_{j-1}, \mathcal{Z}_0 = \mathcal{P}_T(\mathcal{U} \diamond_{\Phi} \mathcal{V}^H). \quad (15)$$

In the following we will show that  $\mathcal{Y}$  defined in (15) satisfies the conditions (13) and (14).

For (13). Set  $\mathcal{D}_k := \mathcal{U} \diamond_{\Phi} \mathcal{V}^H - \mathcal{P}_T(\mathcal{Z}_k)$  for  $k = 0, \dots, k_0$ . By the definition of  $\mathcal{Z}_k$ , we have  $\mathcal{D}_0 = \mathcal{U} \diamond_{\Phi} \mathcal{V}^H$  and

$$\mathcal{D}_k = (\mathcal{P}_T - \mathcal{P}_T \mathcal{P}_{\Omega_k} \mathcal{P}_T) \mathcal{D}_{k-1}. \quad (16)$$

Note that  $\Omega_k$  is independent of  $\mathcal{D}_{k-1}$  and  $q \geq p/k_0 \geq c_0 \mu_0 \sum r_i \log n_{(1)} n_3 / n_{(1)} n_3$ . For each  $k$ , by Lemma 3.3 with  $\Omega$  replaced by  $\Omega_k$ , we have

$$\|\mathcal{D}_k\|_F \leq \|\mathcal{P}_T - \mathcal{P}_T \mathcal{P}_{\Omega_k} \mathcal{P}_T\| \|\mathcal{D}_{k-1}\|_F \leq \frac{1}{2} \|\mathcal{D}_{k-1}\|_F.$$

It follows that

$$\|\mathcal{P}_T(\mathcal{Y}) - \mathcal{U} \diamond_{\Phi} \mathcal{V}^H\|_F = \|\mathcal{D}_{k_0}\|_F \leq \left(\frac{1}{2}\right)^{k_0} \|\mathcal{U} \diamond_{\Phi} \mathcal{V}^H\|_F \leq \frac{1}{4(n_{(1)} n_3)^2} \sqrt{r} \leq \frac{1}{4n_{(1)} n_3^2}.$$

For (14). Note that  $\mathcal{Y} = \sum_{k=1}^{k_0} \mathcal{P}_{\Omega_k} \mathcal{P}_T(\mathcal{D}_{k-1})$  by construction. Thus

$$\|\mathcal{P}_{T^\perp}(\mathcal{Y})\| \leq \sum_{k=1}^{k_0} \|\mathcal{P}_{T^\perp}(\mathcal{P}_{\Omega_k} \mathcal{P}_T - \mathcal{P}_T)(\mathcal{D}_{k-1})\| \leq \sum_{k=1}^{k_0} \|(\mathcal{P}_{\Omega_k} - I) \mathcal{P}_T(\mathcal{D}_{k-1})\|. \quad (17)$$

Applying Lemma 3.4 with  $\Omega$  replaced by  $\Omega_k$  to each summand of (17) yields

$$\begin{aligned} \|\mathcal{P}_{T^\perp}(\mathcal{Y})\| &\leq c \sum_{k=1}^{k_0} \left( \frac{\log n_{(1)} n_3}{q} \|\mathcal{D}_{k-1}\|_\infty + \sqrt{\frac{\log n_{(1)} n_3}{q}} \|\mathcal{D}_{k-1}\|_{\infty,w} \right) \\ &\leq \frac{c}{\sqrt{c_0}} \sum_{k=1}^{k_0} \left( \frac{n_{(1)} n_3}{\mu_0 \sum r_i} \|\mathcal{D}_{k-1}\|_\infty + \sqrt{\frac{n_{(1)} n_3}{\mu_0 \sum r_i}} \|\mathcal{D}_{k-1}\|_{\infty,w} \right). \end{aligned} \quad (18)$$

Using (16), and applying Lemma 3.3 with  $\Omega$  replaced by  $\Omega_k$ , we can get

$$\|\mathcal{D}_{k-1}\|_\infty = \|(\mathcal{P}_{T^\perp}(\mathcal{P}_{\Omega_{k-1}} \mathcal{P}_T - \mathcal{P}_T) \cdots \mathcal{P}_{T^\perp}(\mathcal{P}_{\Omega_1} \mathcal{P}_T - \mathcal{P}_T)) \mathcal{D}_0\|_\infty \leq \frac{1}{2^k} \|\mathcal{U} * \mathcal{V}^H\|_\infty.$$

It follows from Lemma 3.5 that

$$\|\mathcal{D}_{k-1}\|_{\infty,w} = \|(\mathcal{P}_T - \mathcal{P}_T \mathcal{P}_{\Omega_{k-1}} \mathcal{P}_T) \mathcal{D}_{k-2}\|_{\infty,w} \leq \frac{1}{2} \sqrt{\frac{n_{(1)} n_3}{\mu_0 \sum r_i}} \|\mathcal{D}_{k-2}\|_{\infty} + \frac{1}{2} \|\mathcal{D}_{k-2}\|_{\infty,w}$$

holds with high probability. Moreover, it follows (16) that

$$\|\mathcal{D}_{k-1}\|_{\infty,w} \leq \frac{k}{2^{k-1}} \sqrt{\frac{n_{(1)} n_3}{\mu_0 \sum r_i}} \|\mathcal{U} \diamond_{\Phi} \mathcal{V}^H\|_{\infty} + \frac{1}{2^{k-1}} \|\mathcal{U} \diamond_{\Phi} \mathcal{V}^H\|_{\infty,w}.$$

Taking them back to (18) gives

$$\begin{aligned} & \|\mathcal{P}_{T^\perp}(\mathcal{Y})\| \\ & \leq \frac{c}{\sqrt{c_0}} \frac{n_{(1)} n_3}{\mu_0 \sum r_i} \|\mathcal{U} \diamond_{\Phi} \mathcal{V}^H\|_{\infty} \sum_{k=1}^{k_0} (k+1) \left(\frac{1}{2}\right)^{k-1} + \frac{c}{\sqrt{c_0}} \sqrt{\frac{n_{(1)} n_3}{\mu_0 \sum r_i}} \|\mathcal{U} \diamond_{\Phi} \mathcal{V}^H\|_{\infty,w} \sum_{k=1}^{k_0} \left(\frac{1}{2}\right)^{k-1} \\ & \leq \frac{6c}{\sqrt{c_0}} \frac{n_{(1)} n_3}{\mu_0 \sum r_i} \|\mathcal{U} \diamond_{\Phi} \mathcal{V}^H\|_{\infty} + \frac{2c}{\sqrt{c_0}} \sqrt{\frac{n_{(1)} n_3}{\mu_0 \sum r_i}} \|\mathcal{U} \diamond_{\Phi} \mathcal{V}^H\|_{\infty,w}. \end{aligned} \quad (19)$$

By the incoherence conditions given in (7)-(8), we can get

$$\|\mathcal{U} \diamond_{\Phi} \mathcal{V}^H\|_{\infty} \leq \max_{i,j,k} \|\mathcal{U} \diamond_{\Phi} \vec{e}_{ik}\|_F \|\mathcal{V}^H \diamond_{\Phi} \vec{e}_{ik}\|_F \leq \frac{\mu_0 \sum r_i}{n_{(1)} n_3}, \quad (20)$$

$$\|\mathcal{U} \diamond_{\Phi} \mathcal{V}^H\|_{\infty,w} \leq \max \left\{ \max_{i,k} \|\mathcal{U} \diamond_{\Phi} \mathcal{V}^H \diamond_{\Phi} \vec{e}_{ik}\|_F, \max_{j,k} \|\vec{e}_{jk}^H \diamond_{\Phi} \mathcal{U} \diamond_{\Phi} \mathcal{V}^H\|_F \right\} \leq \sqrt{\frac{\mu_0 \sum r_i}{n_{(1)} n_3}}. \quad (21)$$

Plugging (20) and (21) into (19), we obtain that

$$\|\mathcal{P}_{T^\perp}(\mathcal{Y})\| \leq \frac{6c}{\sqrt{c_0}} + \frac{2c}{\sqrt{c_0}} \leq \frac{1}{2}$$

provided  $c_0$  is sufficiently large.

Moreover, for any tensor  $\mathcal{Z} \in \{\mathcal{Z} \in \mathbb{C}^{n_1 \times n_1 \times n_3} | \mathcal{P}_{\Omega}(\mathcal{Z}) = 0\}$ , denote the skinny transformed tensor SVD of  $\mathcal{P}_{T^\perp}(\mathcal{Z})$  by

$$\mathcal{P}_{T^\perp}(\mathcal{Z}) = \mathcal{U}_{\perp} \diamond_{\Phi} \mathcal{S}_{\perp} \diamond_{\Phi} \mathcal{V}_{\perp}^H.$$

Since  $\bar{\mathcal{U}}^H \cdot \bar{\mathcal{U}}_{\perp} = 0$  and  $\bar{\mathcal{V}}^H \cdot \bar{\mathcal{V}}_{\perp} = 0$ , we have

$$\|\mathcal{U} \diamond_{\Phi} \mathcal{V}^H + \mathcal{U}_{\perp} \diamond_{\Phi} \mathcal{V}_{\perp}^H\| = \|\bar{\mathcal{U}} \cdot \bar{\mathcal{V}}^H + \bar{\mathcal{U}}_{\perp} \cdot \bar{\mathcal{V}}_{\perp}^H\| = 1.$$

Thus,

$$\begin{aligned} \|\mathcal{X}_0 + \mathcal{Z}\|_{\text{TTNN}} & \geq \langle \mathcal{U} \diamond_{\Phi} \mathcal{V}^H + \mathcal{U}_{\perp} \diamond_{\Phi} \mathcal{V}_{\perp}^H, \mathcal{X}_0 + \mathcal{Z} \rangle \\ & = \langle \mathcal{U} \diamond_{\Phi} \mathcal{V}^H, \mathcal{X}_0 \rangle + \langle \mathcal{U}_{\perp} \diamond_{\Phi} \mathcal{V}_{\perp}^H, \mathcal{P}_{T^\perp}(\mathcal{Z}) \rangle + \langle \mathcal{U} \diamond_{\Phi} \mathcal{V}^H, \mathcal{Z} \rangle \\ & = \|\mathcal{X}_0\|_{\text{TTNN}} + \|\mathcal{P}_{T^\perp}(\mathcal{Z})\|_{\text{TTNN}} + \langle \mathcal{U} \diamond_{\Phi} \mathcal{V}^H, \mathcal{Z} \rangle \\ & \geq \|\mathcal{X}_0\|_{\text{TTNN}} + \|\mathcal{P}_{T^\perp}(\mathcal{Z})\|_{\text{TTNN}} - |\langle \mathcal{Y} - \mathcal{U} \diamond_{\Phi} \mathcal{V}^H, \mathcal{Z} \rangle - \langle \mathcal{Y}, \mathcal{Z} \rangle| \\ & \geq \|\mathcal{X}_0\|_{\text{TTNN}} + \|\mathcal{P}_{T^\perp}(\mathcal{Z})\|_{\text{TTNN}} - \|\mathcal{P}_{T^\perp}(\mathcal{Y})\| \|\mathcal{P}_{T^\perp}(\mathcal{Z})\|_{\text{TTNN}} \\ & \quad - \|\mathcal{P}_T(\mathcal{Y}) - \mathcal{U} \diamond_{\Phi} \mathcal{V}^H\|_F \|\mathcal{P}_T(\mathcal{Z})\|_F \\ & \geq \|\mathcal{X}_0\|_{\text{TTNN}} + \frac{1}{2} \|\mathcal{P}_{T^\perp}(\mathcal{Z})\|_{\text{TTNN}} - \frac{1}{4n_{(1)} n_3} \|\mathcal{P}_T(\mathcal{Z})\|_F. \end{aligned} \quad (22)$$

Moreover, it follows from Lemma 3.6 that the inequality (22) holds if and only if  $\mathcal{P}_{T^\perp}(\mathcal{Z}) = \mathcal{P}_\Omega(\mathcal{Z}) = 0$ . On the other hand,

$$\|\mathcal{P}_T \mathcal{P}_\Omega\|_{\text{op}} \leq \sqrt{\frac{3\rho}{2}} < 1$$

implies that  $\mathcal{P}_T \mathcal{P}_\Omega$  is injective on  $T$ . Therefore, (22) holds if and only if  $\mathcal{Z} = 0$ . This completes the proof.  $\square$

In the next section, we demonstrate that the theoretical result can be obtained under valid incoherence conditions and the tensor completion performance of the proposed method is better than that of other testing methods.

## 4 Experimental Results

In this section, numerical examples are presented to demonstrate the effectiveness of the proposed model. All numerical experiments are obtained from a desktop computer running on 64-bit Windows Operating System having 8 cores with Intel(R) Core(TM) i7-6700 CPU at 3.40GHz and 20 GB memory.

Firstly, we employ an alternating direction method of multipliers (ADMM) [7, 8] to solve problem (6). Let  $\mathcal{X} = \mathcal{Y}$ . Then problem (6) can be rewritten as

$$\begin{aligned} \min_{\mathcal{X}} \quad & \|\mathcal{X}\|_{\text{TNN}} \\ \text{s.t.} \quad & \mathcal{X} = \mathcal{Y}, \mathcal{P}_\Omega(\mathcal{Y}) = \mathcal{P}_\Omega(\mathcal{M}). \end{aligned} \quad (23)$$

The augmented Lagrangian function associated with (23) is defined by

$$L(\mathcal{X}, \mathcal{Y}, \mathcal{Z}) := \|\mathcal{X}\|_{\text{TNN}} - \langle \mathcal{Z}, \mathcal{X} - \mathcal{Y} \rangle + \frac{\beta}{2} \|\mathcal{X} - \mathcal{Y}\|_F^2, \quad (24)$$

where  $\mathcal{Z}$  is the Lagrangian multiplier and  $\beta > 0$  is the penalty parameter. The ADMM iteration system is given as follows:

$$\mathcal{X}^{k+1} = \arg \min_{\mathcal{X}} \left\{ L(\mathcal{X}, \mathcal{Y}^k, \mathcal{Z}^k) \right\}, \quad (25)$$

$$\mathcal{Y}^{k+1} = \arg \min_{\mathcal{Y}} \left\{ L(\mathcal{X}^{k+1}, \mathcal{Y}, \mathcal{Z}^k) : \mathcal{P}_\Omega(\mathcal{Y}) = \mathcal{P}_\Omega(\mathcal{M}) \right\}, \quad (26)$$

$$\mathcal{Z}^{k+1} = \mathcal{Z}^k - \gamma\beta (\mathcal{X}^{k+1} - \mathcal{Y}^{k+1}), \quad (27)$$

where  $\gamma \in (0, \frac{1+\sqrt{5}}{2})$  is the dual steplength. It follows from [28, Theorem 3] that the optimal solution with respect to (25) is given by

$$\mathcal{X}^{k+1} = \mathcal{U} \diamond_{\Phi} \mathcal{S}_\beta \diamond_{\Phi} \mathcal{V}^H, \quad (28)$$

where  $\mathcal{Y}^k + \frac{1}{\beta} \mathcal{Z}^k = \mathcal{U} \diamond_{\Phi} \mathcal{S} \diamond_{\Phi} \mathcal{V}^H$ ,  $\mathcal{S}_\beta = \Phi^H[\hat{\mathcal{S}}_\beta]$ , and  $\hat{\mathcal{S}}_\beta = \max\{\hat{\mathcal{S}}_\Phi - \frac{1}{\beta}, 0\}$ .

The optimal solution with respect to (26) is given by

$$\mathcal{Y}^{k+1} = \mathcal{P}_{\bar{\Omega}} \left( \mathcal{X}^{k+1} - \frac{1}{\beta} \mathcal{Z}^k \right) + \mathcal{P}_\Omega(\mathcal{M}), \quad (29)$$

where  $\bar{\Omega}$  denotes the complementary set of  $\Omega$  on  $\{1, \dots, n_1\} \times \{1, \dots, n_2\} \times \{1, \dots, n_3\}$ . Then the ADMM for solving (23) can be presented in Algorithm 1.

---

**Algorithm 1** Alternating direction method of multipliers for solving (23)

---

**Step 0.**  $\tau \in (0, (1 + \sqrt{5})/2)$ ,  $\beta > 0$ ,  $\mathcal{Y}^0, \mathcal{Z}^0$ . For  $k = 0, 1, 2, \dots$ , perform the following steps:

**Step 1.** Compute  $\mathcal{X}^{k+1}$  by (28).

**Step 2.** Compute  $\mathcal{Y}^{k+1}$  via (29).

**Step 3.** Compute  $\mathcal{Z}^{k+1}$  by (27).

---

The convergence of a two-block ADMM has been established in [7, Theorem B.1] and the convergence of Algorithm 1 can be derived from this theorem easily. The Karush-Kuhn-Tucker (KKT) conditions of (23) are given as follows:

$$\begin{cases} 0 \in \partial \|\mathcal{X}\|_{\text{TNN}} - \mathcal{Z}, \\ \mathcal{X} = \mathcal{Y}, \mathcal{P}_\Omega(\mathcal{Y}) = \mathcal{P}_\Omega(\mathcal{M}). \end{cases} \quad (30)$$

Based on the KKT conditions (30), we adopt the following relative residual to measure the accuracy of an approximate optimal solution in the numerical experiments:

$$\eta := \max\{\eta_x, \eta_y\},$$

where

$$\eta_x = \frac{\|\mathcal{X} - \text{Prox}_{\|\cdot\|_{\text{TNN}}}(\mathcal{Z} + \mathcal{X})\|_F}{1 + \|\mathcal{Z}\|_F + \|\mathcal{X}\|_F}, \quad \eta_y = \frac{\|\mathcal{X} - \mathcal{Y}\|_F}{1 + \|\mathcal{X}\|_F + \|\mathcal{Y}\|_F}.$$

Here  $\text{Prox}_f(y) := \arg \min_x \{f(x) + \frac{1}{2}\|x - y\|_2\}$ . In the practical implementation, Algorithm 1 will be terminated if  $\eta \leq 10^{-3}$  or if the number of iterations exceeds 600. For  $\gamma$ , we set  $\gamma = 1.618$  for the convergence of ADMM [7] in all experiments. Since the penalty parameter  $\beta$  is not too sensitive to the recovered results, we set  $\beta = 0.05$  in the following experiments. The relative error (Rel) is defined by

$$\text{Rel} := \frac{\|\mathcal{X}_{\text{est}} - \mathcal{X}\|_F}{\|\mathcal{X}\|_F},$$

where  $\mathcal{X}_{\text{est}}$  is the estimated tensor and  $\mathcal{X}$  is the true tensor. To evaluate the performance of the proposed method for real-world tensors, the peak signal-to-noise ratio (PSNR) is used to measure the quality of the estimated tensor, which is defined as follows:

$$\text{PSNR} := 10 \log_{10} \frac{n_1 n_2 n_3 (\mathcal{X}_{\max} - \mathcal{X}_{\min})^2}{\|\mathcal{X}_{\text{est}} - \mathcal{X}\|_F^2},$$

where  $\mathcal{X}_{\max}$  and  $\mathcal{X}_{\min}$  denotes the maximum and minimum entries of  $\mathcal{X}$ , respectively. The structural similarity (SSIM) index [31] is used to measure the quality of the recovered and true images for image quality assessment:

$$\text{SSIM} := \frac{(2\mu_x \mu_y + c_1)(2\sigma_{xy} + c_2)}{(\mu_x^2 + \mu_y^2 + c_1)(\sigma_x^2 + \sigma_y^2 + c_2)},$$

where  $\mu_x, \sigma_x$  are the mean intensities and standard deviation of the original images, respectively,  $\mu_y, \sigma_y$  denote the mean intensities and standard deviation of the recovered images, respectively,  $\sigma_{xy}$  denotes the covariance of the original and recovered images, and  $c_1, c_2 > 0$  are constants. For the real-world tensor data, the SSIM is used to denote the average values of all images.

#### 4.1 Transformations of t-SVD

In this subsection, we use the fast Fourier transform (t-SVD (FFT)) and the discrete cosine transform [22] (t-SVD (DCT)) in the  $\Phi$ -product and transformed tensor SVD. The other case is based on data to construct a unitary transform matrix [28]. Note that we unfold  $\mathcal{A}$  into a matrix  $\mathbf{A}$  along the third-dimension (called t-SVD (data)) and take the singular value decomposition of the unfolding matrix  $\mathbf{A} = \mathbf{U}\mathbf{\Sigma}\mathbf{V}^H$ . Suppose that  $\text{rank}(\mathbf{A}) = k$ . It is interesting to observe that  $\mathbf{U}^H$  is the optimal transformation to obtain a low rank matrix of  $\mathbf{A}$ :

$$\min_{\Phi, \mathbf{B}} \|\Phi \mathbf{A} - \mathbf{B}\|_F^2 \quad \text{s.t.} \quad \text{rank}(\mathbf{B}) = k, \quad \Phi^H \Phi = \Phi \Phi^H = \mathbf{I}.$$

In practice, the initial estimator  $\mathcal{A}$  obtained by t-SVD (DCT) in the tensor completion problem can be used to generate  $\Phi$ .

#### 4.2 Comparison of Incoherence Conditions

In this subsection, we show the incoherence conditions (7) and (8) in Theorem 3.1 and also compare the existing tensor incoherence conditions in [37], which are given by

$$\max_{i=1, \dots, n_1} \|\mathcal{U}^H \diamond_{\Phi} \vec{e}_i\|_F \leq \sqrt{\frac{\mu_{old} r}{n_1}}, \quad (31)$$

$$\max_{j=1, \dots, n_2} \|\mathcal{V}^H \diamond_{\Phi} \vec{e}_j\|_F \leq \sqrt{\frac{\mu_{old} r}{n_2}}, \quad (32)$$

where  $r$  is the tubal rank of the target tensor. For simplicity, the parameter  $\mu$  in (7) and (8) in our proposed conditions is denoted by  $\mu_{new}$  and the parameter in (31) and (32) is denoted by  $\mu_{old}$ . Here we will compare the values of  $\mu_{new}$  and  $\mu_{old}$  for different tensors with different multi-ranks.

The random tensors are generated as follows:  $\mathcal{X} = \mathcal{A} \diamond_{\Phi} \mathcal{B} \in \mathbb{C}^{n_1 \times n_2 \times n_3}$  with different multi-rank  $\mathbf{r}$ , where  $\hat{\mathcal{A}}_{\Phi}^{(i)}$  and  $\hat{\mathcal{B}}_{\Phi}^{(i)}$  are generated by MATLAB commands `randn( $n_1, r_i$ )` and `randn( $n_2, r_i$ )`, and  $r_i$  is the  $i$ th elementary of  $\mathbf{r}$ . Here  $\Phi$  denotes FFT, DCT, and an orthogonal matrix generated by the singular value decomposition of the unfolding matrix from  $\mathcal{X}$  along the third dimension, see Section 4.1. We increase  $\sum_{i=1}^n r_i$  from 10 to 100 with increment 10 and show the pair  $(\mu, \sum_{i=1}^n r_i)$  in Figure 1. 100 test instances are simulated, and the average  $\mu_{new}$  and  $\mu_{old}$  values that the equalities held in the proposed incoherence inequalities in (7) and (8), and the previous inequalities in (31) and (32), are respectively displayed. More precisely, the upper figures of Figure 1 show  $\mu_{new}$  and  $\mu_{old}$  versus different multi-rank values in the first inequalities of the incoherence conditions (7) and (31), respectively. The lower figures of Figure 1 show  $\mu_{new}$  and  $\mu_{old}$  versus different multi-rank in the second inequalities of the incoherence conditions (8) and (32), respectively. In Figure 1, the size of the testing tensors is  $50 \times 50 \times 50$ . It can be seen that  $\mu_{new}$  is slightly smaller than  $\mu_{old}$  for different  $\sum_{i=1}^n r_i$  in the case of t-SVD (FFT). And  $\mu_{new}$  and  $\mu_{old}$  are about the same for different multi-rank in the case of and t-SVD (DCT). The  $\mu_{new}$  is slightly larger than  $\mu_{old}$  for different  $\sum_{i=1}^n r_i$  in the case of t-SVD (data).

Moreover, Figure 2 shows the least number of samples required with respect to different multi-rank values based on  $\mu_{new}$  and  $\mu_{old}$  calculated in Figure 1. It is clear that the least number of samples of Theorem 3.1 (proportional to  $\mu_{new}(\sum_{i=1}^n r_i)n \log(n^2)$ ) for exact recovery is much less than that of [37] (proportional to  $\mu_{old} r n^2 \log(n^2)$ ) for t-SVD (FFT), t-SVD (DCT), and t-SVD (data).

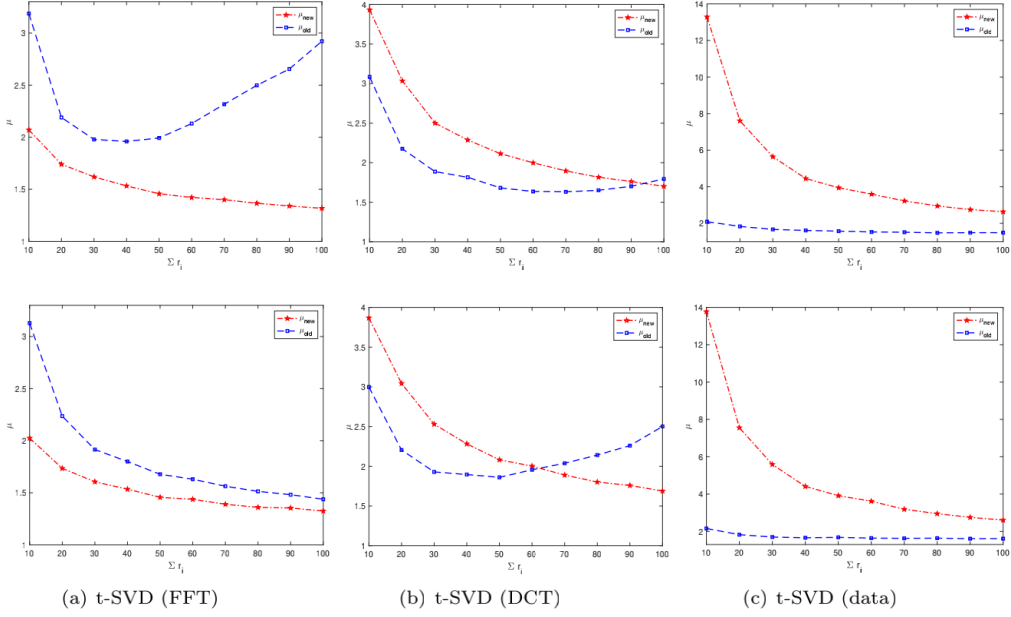


Figure 1:  $\mu$  versus  $\sum_{i=1}^{n_3} r_i$  for the incoherence conditions, where the size of the testing tensor is  $50 \times 50 \times 50$ . First row: The inequality in (7) and (31). Second row: The inequality in (8) and (32).

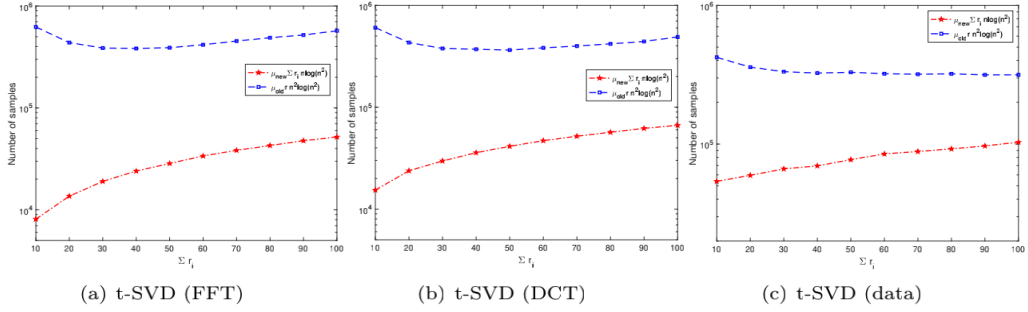


Figure 2: The required number of samples for different  $\mu_{new}$  and  $\mu_{old}$  in Figure 1 with different multi-rank.

Now we consider the tensor with size  $100 \times 100 \times 100$  and increase  $\sum_{i=1}^n r_i$  from 10 to 200 with increment size being 10, where the generated ways of these tensors are the same as those in Figure 1. The results in Figure 3 are similar to those in Figure 1. The parameter value  $\mu_{new}$  is slightly smaller than  $\mu_{old}$  for t-SVD (FFT), they are about the same for t-SVD (DCT), and  $\mu_{old}$  is slightly smaller than  $\mu_{new}$  for t-SVD (data). Again Figure 4 shows the least number of samples for exact tensor completion recovery by the proposed incoherence inequalities (7) and (8), is less than that required by the previous incoherence inequalities [37] in (31) and (32).

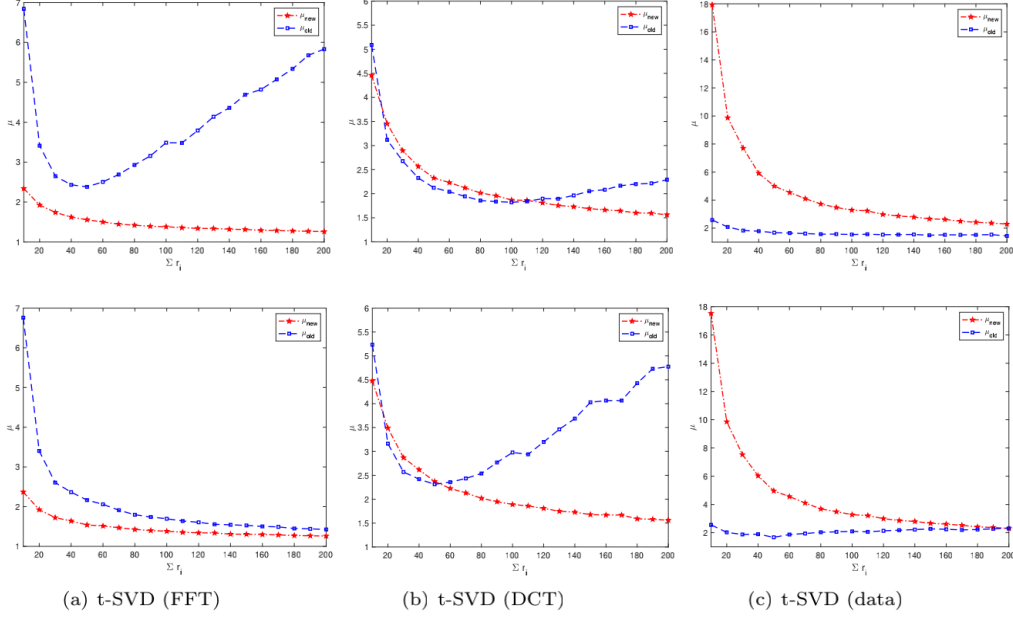


Figure 3:  $\mu$  versus  $\sum_{i=1}^{n_3} r_i$  for the incoherence conditions, where the size of the testing tensor is  $100 \times 100 \times 100$ . First row: The inequality in (7) and (31). Second row: The inequality in (8) and (32).

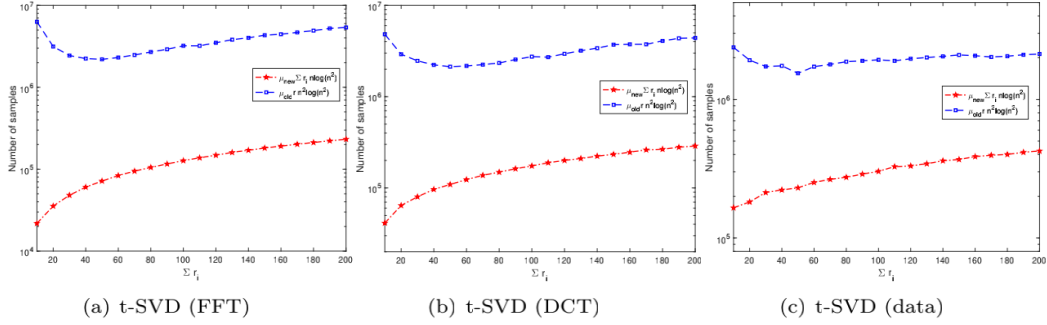


Figure 4: The number of samples for different  $\mu_{new}$  and  $\mu_{old}$  in Figure 3 with different multi-rank.

### 4.3 Recovery Results

In this subsection, we show the recovery results to demonstrate the performance of our analysis for synthetic data and real imaging data sets.

#### 4.3.1 Synthetic Data

With generated tensors in Section 4.2, we check the actual number of samples required for exact tensor recovery with respect to Rel (the relative error). In Figures 5 and 6, we plot the fraction of correct recovery for each pair  $(\sum_{i=1}^n r_i, c)$  for different transforms, where  $c$  refers to the number in samples used in tensor recovery:  $c\mu_{new}n\log(n^2)$ . Here  $\mu_{new}$  are the

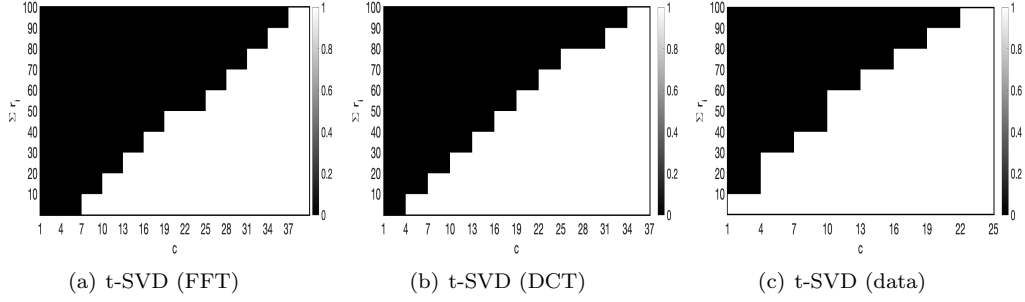


Figure 5: The colormap of different methods for the tensors with size  $50 \times 50 \times 50$ . White denotes the recovery to be successful, and black denotes the recovery to be failed.

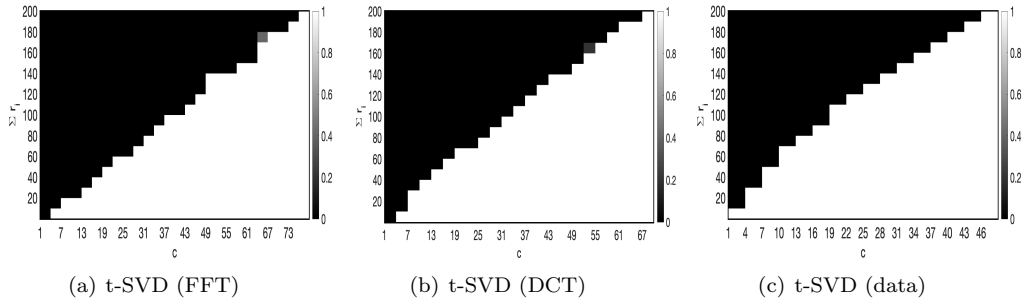


Figure 6: The colormap of different methods for the tensors with size  $100 \times 100 \times 100$ . White denotes perfect recovery, and black denotes failure.

numbers calculated in Figures 1 and 3. For each  $(\sum_{i=1}^n r_i, c)$ -pair, five trials are tested. If Rel is less than  $10^{-2}$  for all five trials, the corresponding tensor recovery is successful (the white region), otherwise it fails (the black region). It is clear from Figures 5 and 6 that when  $c$  is large and/or  $\sum_{i=1}^n r_i$  is small, tensor recovery can be achieved.

In Tables 2 and 3, we display the smallest value of  $c_{small}$  required for successful tensor recovery and the corresponding value of  $\mu_{new}$ , the actual number of samples required ( $c_{small}\mu_{new}n \log(n^2)$ ) and the theoretical number of samples required ( $\mu_{new} \sum_i r_i n \log(n^2)$ ). For comparison, we list the theoretical number of samples required ( $\mu_{old} r n^2 \log(n^2)$ ) by the previous result in [37]. The ratio between  $c_{small}\mu_{new}n \log(n^2)$  and  $\mu_{old} r n^2 \log(n^2)$  is also shown for reference. It is clear from Tables 2 and 3 that the proposed incoherence conditions and the required number of samples for tensor recovery are more effective than the previous method. According to the tables, the number of samples required is about 1% to 5% of the previous estimated sample sizes.

#### 4.3.2 Hyperspectral Images

In this subsection, two hyperspectral datasets (Samson ( $95 \times 95 \times 156$ ) and Japser Ridge ( $100 \times 100 \times 198$ ) [38]) are used to test the effectiveness of our proposed incoherence conditions and the required number of samples for tensor recovery. For Samson data,  $n_1$  and  $n_2$  are equal to 95 and  $n_3$  is equal to 156. For Japser data,  $n_1$  and  $n_2$  are equal to 100 and  $n_3$  is equal



Table 2: The number of samples,  $\mu_{new}$  for successful recovery for t-SVD (FFT) with the tensors in Figure 1, where  $c_{small}$  is the smallest tested value for successful recovery.

| $\sum_{i=1}^{n_3} r_i$  | 10     | 20     | 30     | 40     | 50     | 60     | 70     | 80     | 90     | 100    |
|---|--------|--------|--------|--------|--------|--------|--------|--------|--------|--------|
| $c_{small}$   | 7      | 10     | 13     | 16     | 19     | 25     | 28     | 31     | 34     | 37     |
| $\mu_{new}$   | 1.8965 | 1.6929 | 1.5631 | 1.5394 | 1.5800 | 1.3956 | 1.4585 | 1.5557 | 1.4675 | 1.5325 |
| $c_{small}\mu_{new}n\log(n^2)$                                | 5.19e3 | 6.62e3 | 7.95e3 | 9.63e3 | 1.17e4 | 1.36e4 | 1.59e4 | 1.89e4 | 1.95e4 | 2.22e4 |
| $\mu_{new}\sum r_i n\log(n^2)$                                | 7.42e3 | 1.32e4 | 1.83e4 | 2.41e4 | 3.09e4 | 3.28e4 | 3.99e4 | 4.87e4 | 5.17e4 | 6.00e4 |
| $\mu_{old}$   | 2.6360 | 2.1275 | 1.9900 | 1.9601 | 2.0918 | 1.9517 | 2.4071 | 2.5437 | 2.5612 | 2.7746 |
| $\mu_{old}rn^2\log(n^2)$                                      | 5.16e5 | 4.16e5 | 3.89e5 | 3.83e5 | 4.09e5 | 3.82e5 | 4.71e5 | 4.98e5 | 5.01e5 | 5.43e5 |
| $\frac{c_{small}\mu_{new}n\log(n^2)}{\mu_{old}rn^2\log(n^2)}$ | 0.0101 | 0.0159 | 0.0204 | 0.0251 | 0.0287 | 0.0358 | 0.0339 | 0.0379 | 0.0390 | 0.0409 |

Table 3: The number of samples,  $\mu_{new}$  for successful recovery for t-SVD (FFT) with the tensors in Figure 3, where  $c_{small}$  is the smallest tested value for successful recovery.

| $\sum_{i=1}^{n_3} r_i$  | 10     | 20     | 30     | 40     | 50     | 60     | 70     | 80     | 90     | 100    |
|---|--------|--------|--------|--------|--------|--------|--------|--------|--------|--------|
| $c_{small}$   | 4      | 7      | 13     | 16     | 19     | 22     | 28     | 31     | 34     | 37     |
| $\mu_{new}$   | 2.8497 | 1.8938 | 1.7590 | 1.7156 | 1.6910 | 1.5599 | 1.5570 | 1.4652 | 1.5239 | 1.5057 |
| $c_{small}\mu_{new}n\log(n^2)$                                | 1.05e4 | 1.22e4 | 2.11e4 | 2.53e4 | 2.96e4 | 3.16e4 | 4.02e4 | 4.18e4 | 4.77e4 | 4.79e4 |
| $\mu_{new}\sum r_i n\log(n^2)$                                | 2.63e4 | 3.49e4 | 4.86e4 | 6.32e4 | 7.79e4 | 8.62e4 | 1.00e5 | 1.08e5 | 1.26e5 | 1.29e5 |
| $\mu_{old}$   | 6.1701 | 3.4499 | 3.1190 | 2.4950 | 2.4254 | 2.3610 | 2.8469 | 2.8610 | 3.0959 | 3.3482 |
| $\mu_{old}rn^2\log(n^2)$                                      | 5.68e6 | 3.18e6 | 2.87e6 | 2.30e6 | 2.23e6 | 2.17e6 | 2.62e6 | 2.64e6 | 2.85e6 | 3.08e6 |
| $\frac{c_{small}\mu_{new}n\log(n^2)}{\mu_{old}rn^2\log(n^2)}$ | 0.0032 | 0.0055 | 0.0073 | 0.0110 | 0.0132 | 0.0165 | 0.0153 | 0.0159 | 0.0167 | 0.0155 |
| $\sum_{i=1}^{n_3} r_i$  | 110    | 120    | 130    | 140    | 150    | 160    | 170    | 180    | 190    | 200    |
| $c_{small}$   | 43     | 46     | 49     | 49     | 58     | 64     | 64     | 67     | 73     | 76     |
| $\mu_{new}$   | 1.3455 | 1.3982 | 1.4669 | 1.4924 | 1.3442 | 1.3067 | 1.3664 | 1.4178 | 1.3268 | 1.3173 |
| $c_{small}\mu_{new}n\log(n^2)$                                | 5.33e4 | 5.92e4 | 6.62e4 | 6.74e4 | 7.18e4 | 7.70e4 | 8.04e4 | 8.75e4 | 8.92e4 | 9.22e4 |
| $\mu_{new}\sum r_i n\log(n^2)$                                | 1.36e5 | 1.55e5 | 1.76e5 | 1.92e5 | 1.86e5 | 1.93e5 | 2.14e5 | 2.35e5 | 2.32e5 | 2.43e5 |
| $\mu_{old}$   | 3.2441 | 3.8750 | 3.9150 | 4.3027 | 4.7163 | 4.8107 | 5.0141 | 5.4137 | 5.6706 | 5.6440 |
| $\mu_{old}rn^2\log(n^2)$                                      | 2.99e6 | 3.57e6 | 3.61e6 | 3.96e6 | 4.34e6 | 4.43e6 | 4.62e6 | 4.99e6 | 5.22e6 | 5.20e6 |
| $\frac{c_{small}\mu_{new}n\log(n^2)}{\mu_{old}rn^2\log(n^2)}$ | 0.0178 | 0.0166 | 0.0184 | 0.0170 | 0.0165 | 0.0174 | 0.0174 | 0.0175 | 0.0171 | 0.0177 |

to 198. Here we compare our method with the low-rank tensor completion method using the sum of nuclear norm of unfolding matrices of a tensor (LRTC)<sup>1</sup> [10, 18], tensor factorization method (TF)<sup>2</sup> [12], Square Deal [21], gradient descent algorithm on Grassmannians (GoG) [32]. These testing hyperspectral data is normalized on [0, 1]. Their theoretical estimation of samples required are presented in Table 1.

We remark that these hyperspectral images are not exactly low multi-rank tensors, both the number ( $\mu_{new}$ ) and the multi-rank ( $\sum_{i=1}^{n_3} r_i$ ) are not available. A truncated tensor is used to compute the multi-rank and tubal rank by using the threshold  $\epsilon$ . Here for a given tensor  $\mathcal{X}$  with tensor singular value decomposition in (2) of Theorem 2.2 and  $\epsilon$ , we determine the last value of  $k$  such that

$$\frac{\sum_{i=1}^k \varrho_i}{\sum_{i=1}^{n_{(2)}n_3} \varrho_i} \geq \epsilon,$$

where  $\{\varrho_i\}$  is the sorted value in ascending order of the numbers  $\{\hat{\mathcal{S}}(j, j, \ell)\}_{1 \leq j \leq n_{(2)}, 1 \leq \ell \leq n_3}$  appearing in the diagonal tensor  $\mathcal{S}$  in (2). The ratio is used to determine the significant numbers are kept in the truncated tensor based on the threshold  $\epsilon$ . Now we can define the

<sup>1</sup><http://www.cs.rochester.edu/~jliu/>

<sup>2</sup><https://homes.cs.washington.edu/~sewoong/papers.html>

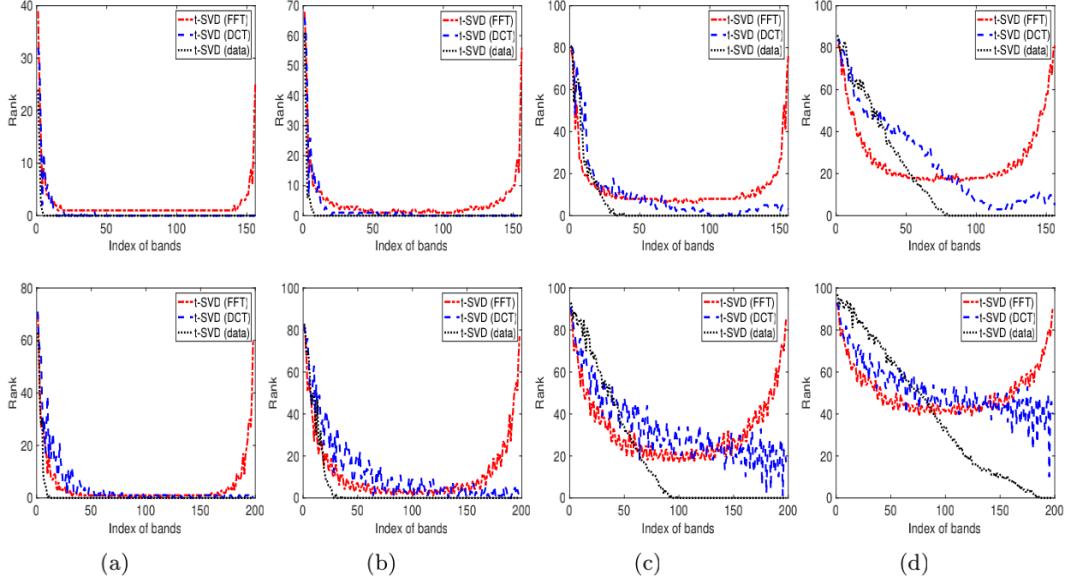


Figure 7: The distribution of multi-ranks of the hyperspectral data sets with different truncations in each band. First row: Samson dataset. Second row: Japser Ridge dataset. (a)  $\epsilon = 70\%$ . (b)  $\epsilon = 80\%$ . (c)  $\epsilon = 90\%$ . (d)  $\epsilon = 95\%$ .

Table 4: The ratios between  $\sum_{i=1}^{n_3} r_i(\epsilon)$  and  $r(\epsilon)$  for the two hyperspectral data sets with different transforms.

| $\epsilon$ | Samson      |             |              | Japser Ridge |             |              |
|------------|-------------|-------------|--------------|--------------|-------------|--------------|
|            | t-SVD (FFT) | t-SVD (DCT) | t-SVD (data) | t-SVD (FFT)  | t-SVD (DCT) | t-SVD (data) |
| 70%        | 0.0567      | 0.0260      | 0.0107       | 0.0675       | 0.0626      | 0.0189       |
| 80%        | 0.0721      | 0.0330      | 0.0123       | 0.1497       | 0.1489      | 0.0528       |
| 90%        | 0.1745      | 0.1282      | 0.0673       | 0.3648       | 0.3657      | 0.2066       |
| 95%        | 0.3515      | 0.3125      | 0.2193       | 0.5504       | 0.5540      | 0.3987       |

multi-rank  $\mathbf{r}(\epsilon)$  of the truncated tensor as follows:

$$\mathbf{r}(\epsilon) := (r_1(\epsilon), \dots, r_{n_3}(\epsilon)), \text{ with } r_\ell(\epsilon) := \#\{\hat{\mathcal{S}}(j, j, \ell) \geq \varrho_k, 1 \leq j \leq n_{(2)}\}, \ell = 1, \dots, n_3,$$

Accordingly, the tubal rank of the truncated tensor is defined as  $r(\epsilon) := \max\{r_1(\epsilon), \dots, r_{n_3}(\epsilon)\}$ . The distributions of the multi-ranks of the two hyperspectral data sets with different  $\epsilon$  are shown in Figure 7. It can be seen that the  $\sum_{i=1}^{n_3} r_i(\epsilon)$  obtained by t-SVD (data) is smaller than that obtained by t-SVD (FFT) and t-SVD (DCT) for different truncations  $\epsilon = 70\%, 80\%, 90\%, 95\%$ , which implies that the t-SVD (data) needs lower number of samples for successful recovery than t-SVD (FFT) and t-SVD (DCT). The distributions of multi-ranks of the truncated tensor obtained by t-SVD (FFT) are symmetric due to symmetry of FFT. Furthermore, we show the ratio between the multi-rank ( $\sum_{i=1}^{n_3} r_i(\epsilon)$ ) and the tubal rank ( $r(\epsilon)n_3$ ) for the hyperspectral data in Table 4. It can be seen that the ratio obtained by t-SVD (data) is much smaller than those of t-SVD (FFT) and t-SVD (DCT), which implies that the sample sizes required by t-SVD (data) are smaller than those required by t-SVD (FFT) and t-SVD (DCT).

In Table 5, we present the number of samples ( $const n_1 \log(n_1 n_3)$ ) for several values of  $const$  and their corresponding PSNR and SSIM values of the recovered tensors by different

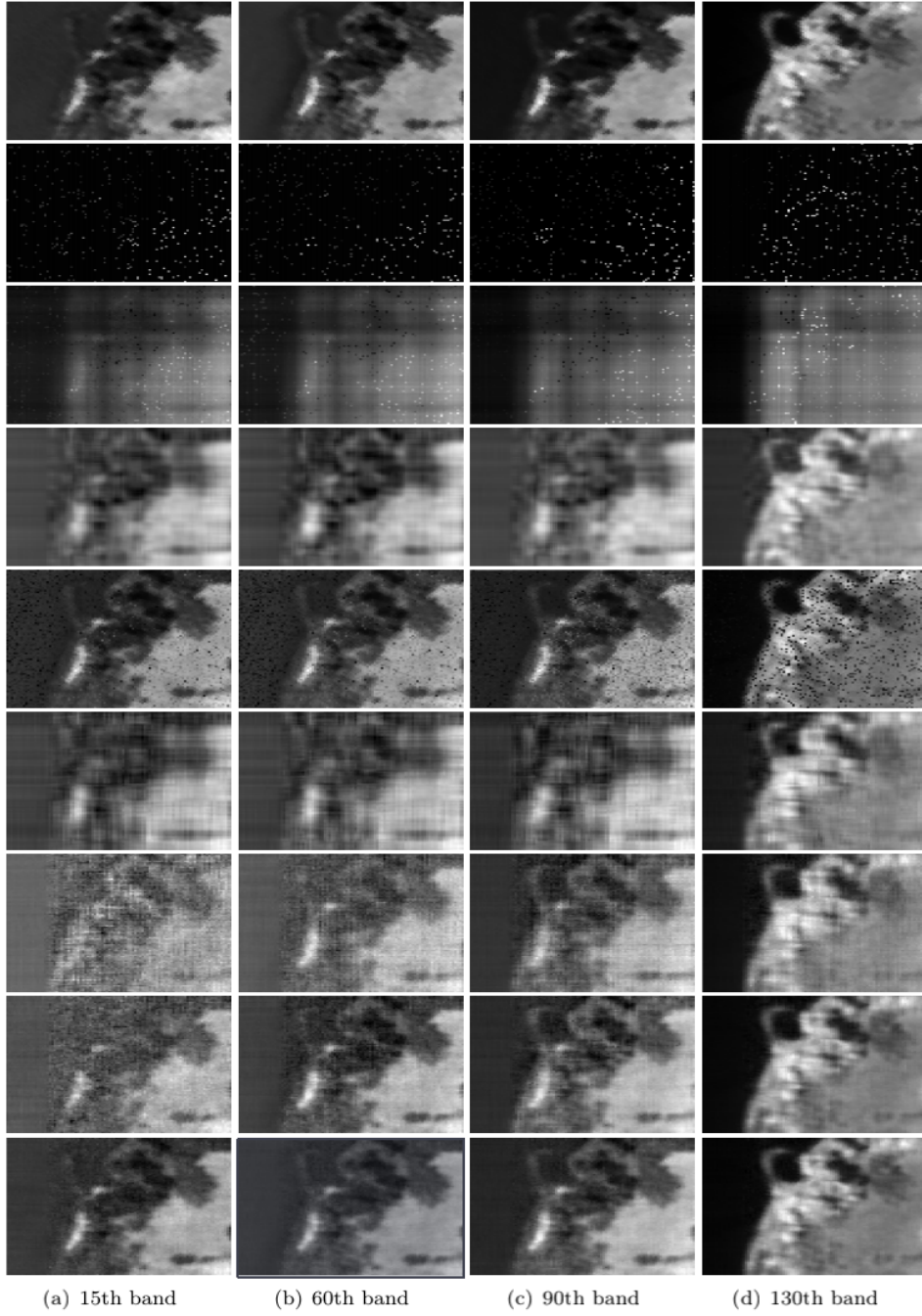


Figure 8: Recovery results by different methods for the Samson data with  $const = 60$ . First row: Original images. Second row: Observed images. Third row: Recovered images by LRTC. Fourth row: Recovered images by TF. Fifth row: Recovered images by Square Deal. Sixth row: Recovered images by GoG. Seventh row: Recovered images by t-SVD (FFT). Eighth row: Recovered images by t-SVD (DCT). Ninth row: Recovered images by t-SVD (data).

Table 5: The PSNR, SSIM values, and CPU time (in seconds) of different methods for the hyper-spectral images.

|              | <i>const</i> | Samson       |              |              |              |              | Japser Ridge |              |              |              |              |
|--------------|--------------|--------------|--------------|--------------|--------------|--------------|--------------|--------------|--------------|--------------|--------------|
|              |              | 20           | 30           | 40           | 50           | 60           | 20           | 30           | 40           | 50           | 60           |
| LRTC         | PSNR         | 13.08        | 16.00        | 18.34        | 19.82        | 20.99        | 12.48        | 14.80        | 16.78        | 18.17        | 18.97        |
|              | SSIM         | 0.3254       | 0.5720       | 0.6223       | 0.6643       | 0.6964       | 0.3245       | 0.4104       | 0.4404       | 0.4611       | 0.4793       |
|              | CPU          | 26.44        | 29.81        | 29.50        | 27.13        | 25.50        | 39.54        | 39.98        | 42.73        | 39.81        | 36.51        |
| TF           | PSNR         | 4.05         | 7.45         | 20.26        | 29.78        | 32.86        | 7.12         | 11.41        | 12.09        | 15.39        | 27.03        |
|              | SSIM         | 0.3990       | 0.4852       | 0.7798       | 0.8627       | 0.8856       | 0.2076       | 0.3728       | 0.6120       | 0.6418       | 0.7246       |
|              | CPU          | 207.55       | 207.20       | 206.90       | 206.80       | 216.99       | 400.27       | 399.79       | 398.94       | 398.46       | 286.83       |
| Square Deal  | PSNR         | 16.35        | 18.55        | 20.38        | 22.15        | 23.77        | 15.38        | 17.50        | 20.47        | 22.48        | 24.25        |
|              | SSIM         | 0.4502       | 0.5727       | 0.6696       | 0.7269       | 0.7916       | 0.3890       | 0.5168       | 0.6199       | 0.7021       | 0.7596       |
|              | CPU          | 37.46        | 34.93        | 33.05        | 30.96        | 29.48        | 43.33        | 41.89        | 41.82        | 41.99        | 40.65        |
| GoG          | PSNR         | 16.72        | 26.02        | 27.13        | 30.01        | 30.45        | 15.32        | 22.38        | 23.54        | 24.35        | 25.44        |
|              | SSIM         | 0.4851       | 0.6978       | 0.7560       | 0.8372       | 0.8366       | 0.2643       | 0.5430       | 0.5624       | 0.5835       | 0.6550       |
|              | CPU          | 1.05e4       | 1.40e4       | 3.41e4       | 3.87e4       | 4.61e4       | 3.49e4       | 4.13e4       | 5.33e4       | 5.50e4       | 5.58e4       |
| t-SVD (FFT)  | PSNR         | 22.09        | 23.88        | 25.21        | 26.27        | 27.09        | 21.04        | 22.95        | 24.09        | 25.17        | 26.06        |
|              | SSIM         | 0.5743       | 0.6498       | 0.6996       | 0.7442       | 0.7689       | 0.4877       | 0.5802       | 0.6353       | 0.6891       | 0.7270       |
|              | CPU          | 30.24        | 26.30        | 25.11        | 24.07        | 22.45        | 50.54        | 42.01        | 37.62        | 35.38        | 34.36        |
| t-SVD (DCT)  | PSNR         | 26.35        | 28.72        | 30.42        | 31.92        | 33.03        | 21.93        | 23.40        | 24.48        | 25.49        | 26.36        |
|              | SSIM         | 0.7355       | 0.8098       | 0.8552       | 0.8875       | 0.9096       | 0.5206       | 0.5945       | 0.6481       | 0.7015       | 0.7378       |
|              | CPU          | 172.41       | 167.56       | 177.44       | 185.69       | 193.36       | 200.90       | 171.96       | 164.15       | 169.65       | 172.05       |
| t-SVD (data) | PSNR         | <b>28.24</b> | <b>31.37</b> | <b>33.39</b> | <b>35.25</b> | <b>36.53</b> | <b>23.54</b> | <b>25.63</b> | <b>27.47</b> | <b>28.74</b> | <b>30.09</b> |
|              | SSIM         | 0.8324       | 0.8971       | 0.9311       | 0.9539       | 0.9643       | 0.6004       | 0.7041       | 0.7816       | 0.8323       | 0.8675       |
|              | CPU          | 241.48       | 258.86       | 270.17       | 282.82       | 284.68       | 235.74       | 217.07       | 217.13       | 230.64       | 235.28       |

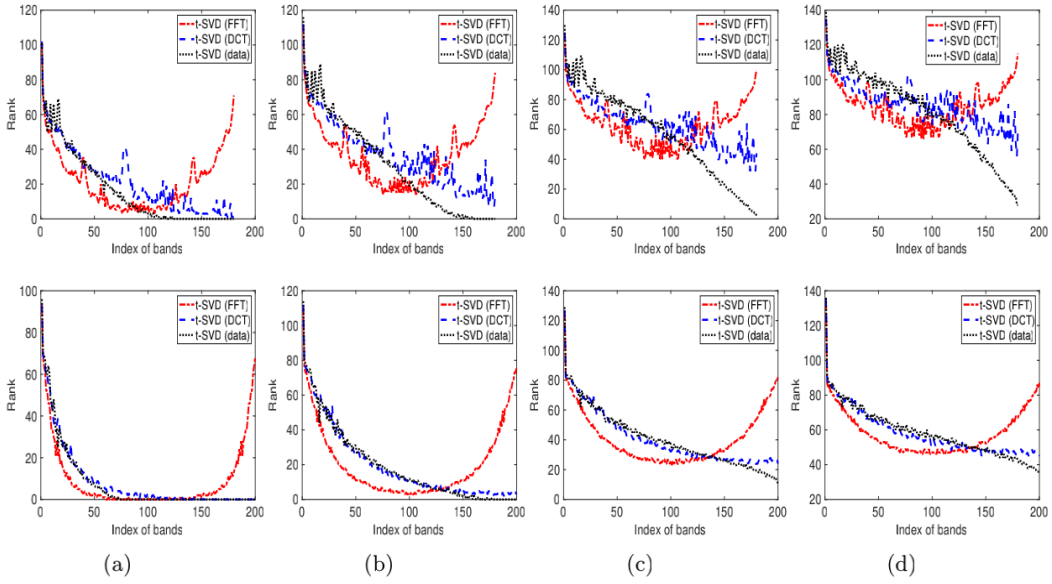


Figure 9: The distribution of multi-ranks of the video data sets with different truncations in each frame. First row: Carphone dataset. Second row: Announcer dataset. (a)  $\epsilon = 70\%$ . (b)  $\epsilon = 80\%$ . (c)  $\epsilon = 90\%$ . (d)  $\epsilon = 95\%$ .

methods. Here we can regard  $const$  as  $c_0\mu \sum_{i=1}^{n_3} r_i(\epsilon)$  in (10) of Theorem 3.1. For  $\epsilon = 70\%$ , the values  $\sum_{i=1}^{n_3} r_i(\epsilon)$  of Samson hyperspectral image are 345, 130, 40 for t-SVD (FFT), t-SVD (DCT), and t-SVD (data), respectively. Thus, the chosen  $const$  is proportional to  $\sum_{i=1}^{n_3} r_i(\epsilon)$  for the testing tensor of hyperspectral image with approximately low multi-rank. We see from the table that for different values of  $const$ , the PSNR and SSIM values obtained

Table 6: The ratios between  $\sum_{i=1}^{n_3} r_i(\epsilon)$  and  $r(\epsilon)$  for the two video data sets with different transforms.

| $\epsilon$ | Carphone    |             |              | Announcer   |             |              |
|------------|-------------|-------------|--------------|-------------|-------------|--------------|
|            | t-SVD (FFT) | t-SVD (DCT) | t-SVD (data) | t-SVD (FFT) | t-SVD (DCT) | t-SVD (data) |
| 70%        | 0.2173      | 0.2133      | 0.1625       | 0.1004      | 0.0887      | 0.0782       |
| 80%        | 0.3370      | 0.3328      | 0.2626       | 0.1865      | 0.1719      | 0.1669       |
| 90%        | 0.5102      | 0.5050      | 0.4386       | 0.3262      | 0.3159      | 0.3118       |
| 95%        | 0.6325      | 0.6317      | 0.5834       | 0.4368      | 0.4286      | 0.4271       |

by t-SVD (data) and t-SVD (DCT) are higher than those obtained by LRTC, TF, Square Deal, GoG, and t-SVD (FFT). For Samson data, the performance of GoG is better than that of t-SVD (FFT) for  $const \geq 30$ . But the computational time required by GoG is significantly more than that required by the other methods. For Japser Ridge data, the PSNR and SSIM values obtained by all three t-SVD methods are almost higher than those obtained by LRTC, TF, Square Deal, and GoG. Moreover, the computational time required by t-SVD methods are quite efficient compared with the other methods.

Figure 8 shows the visual comparisons of different bands by LRTC, TF, Square Deal, GoG, and three t-SVD methods for the Samson data, where  $const = 60$ . We can see that the t-SVD (data) and t-SVD (DCT) outperforms LRTC, TF, Square Deal, and t-SVD (FFT) in terms of visual quality. Moreover, the images recovered by t-SVD (data) keep more details than those recovered by LRTC, TF, Square Deal, t-SVD (FFT), and t-SVD (DCT).

#### 4.3.3 Video Data

In this subsection, we test two video datasets (length  $\times$  width  $\times$  frames) to show the performance of the proposed method, where the testing videos include Carphone ( $144 \times 176 \times 180$ ) and Announcer ( $144 \times 176 \times 200$ )<sup>3</sup>, and we just use the first channels of all frames in the original data. Moreover, the first 180 and 200 frames for these videos are chosen to improve the computational time. The intensity range of the video images is scaled into  $[0, 1]$ .

Similar to Section 4.3.2, the video data sets are not low-rank exactly. First, we show the distributions of multi-ranks with different transformations and  $\epsilon$  in Figure 9. It can be observed that the  $\sum_{i=1}^{n_3} r_i(\epsilon)$  obtained by t-SVD (data) is much smaller than that obtained by t-SVD (FFT) and t-SVD (DCT) for different  $\epsilon$ . Therefore, the number of samples required by t-SVD (data) would be smaller than that required by t-SVD (FFT) and t-SVD (DCT) for the same performance. The distributions of multi-ranks obtained by t-SVD (FFT) are symmetric for different  $\epsilon$  since the FFT has symmetric property. Moreover, we show the ratios between multi-rank ( $\sum_{i=1}^{n_3} r_i(\epsilon)$ ) and tubal rank ( $r(\epsilon)n_3$ ) for several values of  $\epsilon$  for the two videos data sets in Table 6. We can observe that the ratios obtained by t-SVD (data) are smaller than those obtained by t-SVD (FFT) and t-SVD (DCT), especially for small  $\epsilon$ , e.g.,  $\epsilon = 70\%$ . And the  $\sum_{i=1}^{n_3} r_i(\epsilon)$  obtained by t-SVD (DCT) is slightly smaller than that obtained by t-SVD (FFT) for different  $\epsilon$ . The ratios are all smaller than 1 for different  $\epsilon$  in Table 6, which implies that the required number of samples in Theorem 3.1 is smaller than that in [37] for the two approximately low multi-rank tensors.

We use  $const n_{(1)} \log(n_{(1)} n_3)$  number of samples based on Theorem 3.1. The range  $const$  is from 20 to 100 with increment step-size being 10. For example, when  $\epsilon = 70\%$ , the  $\sum_{i=1}^{n_3} r_i(\epsilon)$  of Announcer obtained by t-SVD (FFT), t-SVD (DCT), t-SVD (data) are 1981, 1650, 1502, respectively. When  $const$  is equal to 100, the required sample size would be enough for successful recovery by Theorem 3.1. In this case, the value of  $c_0 \mu_{new}$  in (10) of

<sup>3</sup><https://media.xiph.org/video/derf/>

Table 7: The PSNR, SSIM values, and CPU time (in seconds) of different methods for the video data sets.

|           |              | <i>const</i> | 20           | 30           | 40           | 50           | 60           | 70           | 80           | 90           | 100          |
|-----------|--------------|--------------|--------------|--------------|--------------|--------------|--------------|--------------|--------------|--------------|--------------|
| Carphone  | LRTC         | PSNR         | 10.81        | 11.65        | 12.49        | 13.19        | 13.97        | 14.75        | 15.40        | 16.01        | 16.53        |
|           |              | SSIM         | 0.3498       | 0.3571       | 0.3687       | 0.3870       | 0.4085       | 0.4319       | 0.4496       | 0.4701       | 0.4862       |
|           |              | CPU          | 90.78        | 85.06        | 85.92        | 85.12        | 89.76        | 92.28        | 91.70        | 90.47        | 92.91        |
|           | TF           | PSNR         | 4.96         | 4.64         | 13.41        | 12.98        | 20.82        | 22.57        | 22.66        | 22.74        | 22.75        |
|           |              | SSIM         | 0.2855       | 0.4507       | 0.5081       | 0.5499       | 0.5837       | 0.6461       | 0.6531       | 0.6607       | 0.6622       |
|           |              | CPU          | 780.55       | 779.63       | 771.43       | 782.11       | 762.25       | 770.57       | 771.03       | 765.42       | 760.32       |
|           | Square Deal  | PSNR         | 10.04        | 12.99        | 13.55        | 15.00        | 16.98        | 17.15        | 18.10        | 19.15        | 20.42        |
|           |              | SSIM         | 0.1796       | 0.2675       | 0.3304       | 0.3988       | 0.4497       | 0.4930       | 0.5348       | 0.5719       | 0.6113       |
|           |              | CPU          | 76.98        | 80.23        | 76.06        | 77.03        | 76.76        | 76.36        | 74.78        | 80.00        | 78.59        |
|           | GoG          | PSNR         | 18.59        | 20.18        | 20.77        | 20.46        | 21.22        | 21.35        | 21.48        | 22.11        | 22.47        |
|           |              | SSIM         | 0.4010       | 0.4653       | 0.5229       | 0.5023       | 0.5449       | 0.5483       | 0.5547       | 0.5768       | 0.5874       |
|           |              | CPU          | 1.09e5       | 2.27e5       | 1.30e5       | 1.40e5       | 2.47e5       | 6.27e5       | 3.76e5       | 6.71e5       | 6.32e5       |
|           | t-SVD (FFT)  | PSNR         | 9.79         | 11.55        | 15.06        | 18.53        | 22.04        | 22.59        | 23.07        | 23.38        | 23.72        |
|           |              | SSIM         | 0.1814       | 0.2463       | 0.3759       | 0.4899       | 0.6121       | 0.6367       | 0.6566       | 0.6690       | 0.6816       |
|           |              | CPU          | 53.78        | 58.69        | 77.43        | 88.78        | 107.26       | 103.15       | 98.25        | 93.03        | 88.88        |
|           | t-SVD (DCT)  | PSNR         | 20.24        | 21.18        | 21.93        | 22.42        | 22.91        | 23.24        | 23.60        | 23.87        | 24.15        |
|           |              | SSIM         | 0.5230       | 0.5720       | 0.6044       | 0.6286       | 0.6506       | 0.6642       | 0.6772       | 0.6890       | 0.6484       |
|           |              | CPU          | 323.11       | 291.24       | 271.55       | 251.17       | 237.77       | 226.54       | 214.85       | 205.35       | 198.58       |
|           | t-SVD (data) | PSNR         | <b>20.39</b> | <b>21.43</b> | <b>22.30</b> | <b>22.87</b> | <b>23.45</b> | <b>23.75</b> | <b>24.23</b> | <b>24.56</b> | <b>24.85</b> |
|           |              | SSIM         | 0.5294       | 0.5841       | 0.6236       | 0.6499       | 0.6747       | 0.6877       | 0.7063       | 0.7200       | 0.7298       |
|           |              | CPU          | 366.20       | 337.21       | 314.40       | 293.42       | 278.06       | 261.55       | 253.14       | 242.91       | 235.86       |
| Announcer | LRTC         | PSNR         | 12.72        | 14.03        | 15.28        | 16.42        | 17.76        | 18.83        | 19.88        | 20.74        | 21.46        |
|           |              | SSIM         | 0.4727       | 0.4900       | 0.5087       | 0.5336       | 0.5601       | 0.5869       | 0.6120       | 0.6341       | 0.6520       |
|           |              | CPU          | 100.75       | 96.25        | 100.67       | 103.05       | 104.02       | 105.00       | 104.68       | 103.02       | 100.29       |
|           | TF           | PSNR         | 4.39         | 9.99         | 11.36        | 15.48        | 24.12        | 25.65        | 26.22        | 26.28        | 27.99        |
|           |              | SSIM         | 0.4229       | 0.6176       | 0.6599       | 0.6743       | 0.7076       | 0.7363       | 0.7534       | 0.7544       | 0.8169       |
|           |              | CPU          | 887.20       | 862.11       | 872.41       | 874.64       | 869.01       | 864.04       | 822.11       | 835.96       | 858.93       |
|           | Square Deal  | PSNR         | 11.50        | 14.61        | 16.71        | 19.36        | 20.86        | 23.34        | 24.15        | 24.27        | 26.76        |
|           |              | SSIM         | 0.1692       | 0.2702       | 0.3780       | 0.5004       | 0.6207       | 0.6950       | 0.7488       | 0.7928       | 0.8394       |
|           |              | CPU          | 86.39        | 87.33        | 80.39        | 78.26        | 77.23        | 77.46        | 80.36        | 80.28        | 81.06        |
|           | GoG          | PSNR         | 21.85        | 23.59        | 23.72        | 24.80        | 24.96        | 25.42        | 26.20        | 26.87        | 27.14        |
|           |              | SSIM         | 0.5113       | 0.5854       | 0.6144       | 0.6691       | 0.6775       | 0.6976       | 0.7183       | 0.7566       | 0.7977       |
|           |              | CPU          | 1.94e5       | 2.31e5       | 2.60e5       | 3.54e5       | 6.09e5       | 6.36e5       | 5.49e5       | 5.98e5       | 5.90e5       |
|           | t-SVD (FFT)  | PSNR         | 11.01        | 16.64        | 27.03        | 27.98        | 28.63        | 29.11        | 29.46        | 29.83        | 30.12        |
|           |              | SSIM         | 0.2606       | 0.5339       | 0.8125       | 0.8380       | 0.8564       | 0.8686       | 0.8776       | 0.8865       | 0.8922       |
|           |              | CPU          | 61.87        | 97.82        | 153.63       | 144.82       | 132.18       | 125.67       | 118.75       | 106.63       | 103.44       |
|           | t-SVD (DCT)  | PSNR         | 26.06        | 27.12        | 27.92        | 28.58        | 29.16        | 29.58        | 29.95        | 30.32        | 30.69        |
|           |              | SSIM         | 0.7645       | 0.8078       | 0.8353       | 0.8875       | 0.8703       | 0.8798       | 0.8893       | 0.8985       | 0.9046       |
|           |              | CPU          | 537.80       | 466.05       | 432.45       | 407.57       | 377.23       | 350.59       | 329.40       | 298.93       | 287.79       |
|           | t-SVD (data) | PSNR         | <b>26.08</b> | <b>27.25</b> | <b>28.12</b> | <b>28.76</b> | <b>29.41</b> | <b>29.88</b> | <b>30.24</b> | <b>30.71</b> | <b>31.14</b> |
|           |              | SSIM         | 0.7649       | 0.8113       | 0.8399       | 0.8581       | 0.8741       | 0.8838       | 0.8941       | 0.9037       | 0.9106       |
|           |              | CPU          | 608.38       | 531.39       | 472.35       | 460.30       | 425.59       | 395.42       | 353.94       | 341.43       | 330.40       |

Theorem 3.1 can be less than 0.5. In Table 7, we show the PSNR, SSIM values, and CPU time (in seconds) of different methods for the testing video data sets with different *const*. It can be seen that the performance of t-SVD (data) is better than that of LRTC, TF, Square Deal, GoG, t-SVD (FFT), and t-SVD (DCT) in terms of PSNR and SSIM values. The PSNR and SSIM values obtained by t-SVD (DCT) is higher than those obtained by t-SVD (FFT). Hence, the number of samples required by t-SVD (DCT) and t-SVD (data) is smaller than that required by LRTC, TF, Square Deal, GoG, and t-SVD (FFT) for the same recovery performance, which demonstrates the conclusion of Theorem 3.1. Moreover, the CPU time (in seconds) required by GoG is much more than that required by other methods.

Figure 10 shows the visual quality of the 20th, 80th, 120th, 180th frames of the recovered images by LRTC, TF, Square Deal, GoG, and three t-SVD methods, where *const* = 80. It can be seen that the three t-SVD methods outperform LRTC, TF, Square Deal, and GoG for different frames in terms of visual quality.



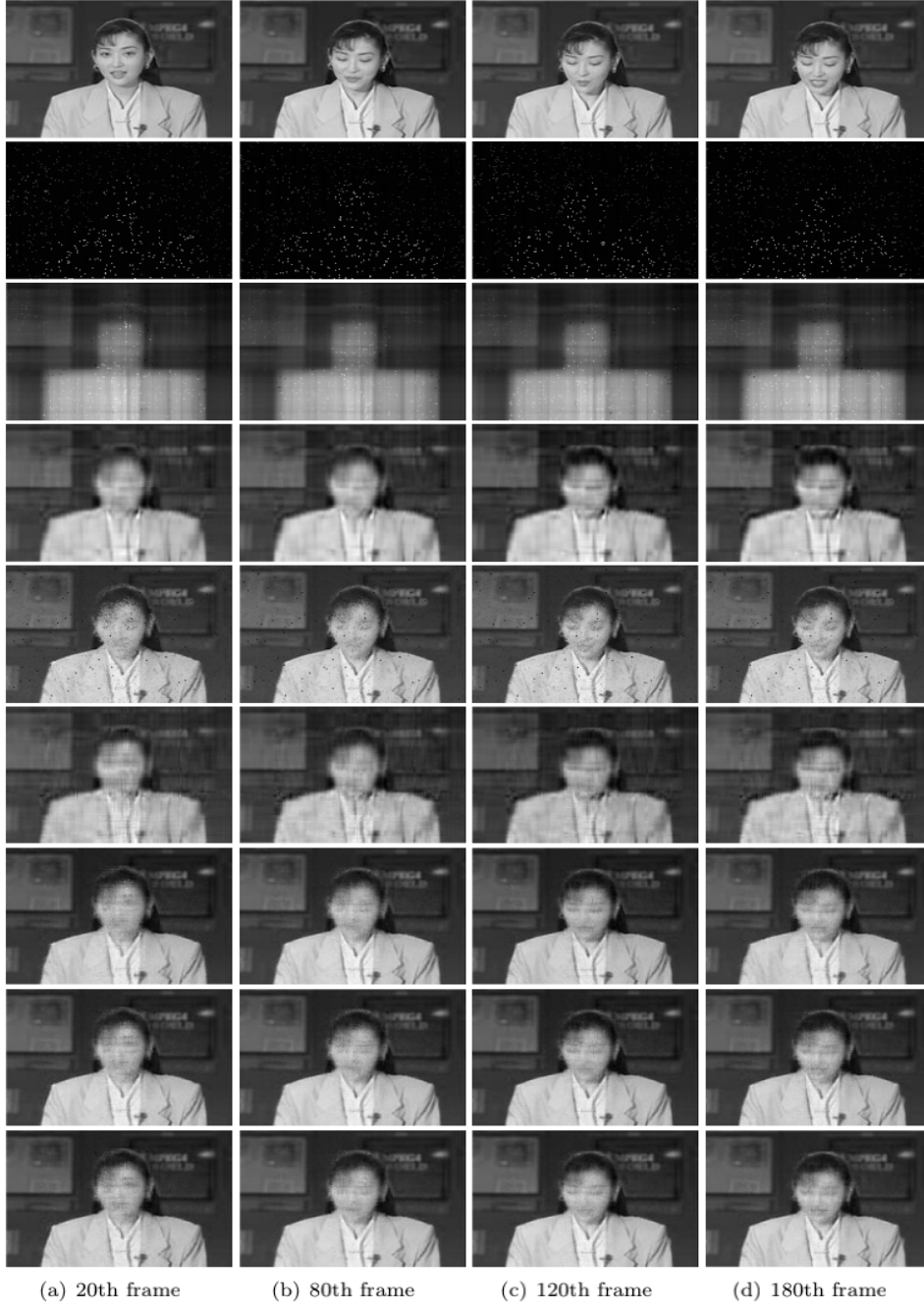


Figure 10: Recovery results by different methods for the Announcer data with  $const = 80$ . First row: Original images. Second row: Observed images. Third row: Recovered images by LRTC. Fourth row: Recovered images by TF. Fifth row: Recovered images by Square Deal. Sixth row: Recovered images by GoG. Seventh row: Recovered images by t-SVD (FFT). Eighth row: Recovered images by t-SVD (DCT). Ninth row: Recovered images by t-SVD (data).

## 5 Concluding Remarks

In this paper, we have established the sample size requirement for exact recovery in the tensor completion problem by using transformed tensor singular value decomposition. We have shown that for any  $\mathcal{X} \in \mathbb{C}^{n_1 \times n_2 \times n_3}$  with transformed multi-rank  $(r_1, r_2, \dots, r_{n_3})$ , one can recover the tensor exactly with high probability under some incoherence conditions if the sample size of observations is of the order  $O(\sum_{i=1}^{n_3} r_i \max\{n_1, n_2\} \log(\max\{n_1, n_2\} n_3))$  under uniformly sampled entries. The sample size requirement of our theory for exact recovery is smaller than that of existing methods for tensor completion. Moreover, several numerical experiments both on synthetic data and real-world data sets are presented to show the superior performance of our methods in comparison with other state-of-the-art methods.

In further work, it would be of great interest to extend the transformed tensor singular value decomposition and tensor completion results to higher-order tensors (cf. [19]).

## Acknowledgments

The authors are grateful to Dr. Cun Mu at Walmart Labs and Dr. Dong Xia at The Hong Kong University of Science and Technology for sharing the codes of the Square Deal [21] and GoG methods [32], respectively.

## 6 Appendix

We first list the following lemma, which is the main tool to prove our conclusions.

**Lemma 6.1.** ([24, Theorem 4]) *Let  $X_1, \dots, X_L \in \mathbb{R}^{n \times n}$  be independent zero mean random matrices of dimension  $d_1 \times d_2$ . Suppose  $\rho_k^2 = \max\{\|\mathbb{E}[X_k X_k^T]\|, \|\mathbb{E}[X_k^T X_k]\|\}$  and  $\|X_k\| \leq B$  almost surely for all  $k$ . Then for any  $\tau > 0$ ,*

$$\mathbb{P}\left[\left\|\sum_{k=1}^L X_k\right\| > \tau\right] \leq (d_1 + d_2) \exp\left(\frac{-\tau^2/2}{\sum_{k=1}^L \rho_k^2 + B\tau/3}\right).$$

Moreover, if  $\max\left\{\left\|\sum_{k=1}^L X_k X_k^T\right\|, \sum_{k=1}^L \|X_k^T X_k\|\right\} \leq \sigma^2$  then for any  $c > 1$ , we have

$$\left\|\sum_{k=1}^L X_k\right\| \leq \sqrt{4c\sigma^2 \log(d_1 + d_2)} + cB \log(d_1 + d_2),$$

with probability at least  $1 - (d_1 + d_2)^{-(c-1)}$ .

### 6.1 Proof of Lemma 3.3

Let  $\mathcal{E}_{ijk}$  be a unit tensor whose  $(i, j, k)$ -th entry is 1 and others are 0. Then for an arbitrary tensor  $\mathcal{Z} \in \mathbb{C}^{n_1 \times n_2 \times n_3}$ , we have  $\mathcal{Z} = \sum_{ijk} \langle \mathcal{E}_{ijk}, \mathcal{Z} \rangle \mathcal{E}_{ijk}$ . Recall Definition 2.7,  $\mathcal{E}_{ijk}$  can be expressed as  $\mathcal{E}_{ijk} = \vec{e}_{ik} \diamond_{\Phi} \vec{e}_{kt} \diamond_{\Phi} \vec{e}_{jk}^H$ , then  $\mathcal{P}_T(\mathcal{Z})$  can also be decomposed as

$$\mathcal{P}_T(\mathcal{Z}) = \sum_{i,j,k} \langle \mathcal{P}_T(\mathcal{Z}), \vec{e}_{ik} \diamond_{\Phi} \vec{e}_{kt} \diamond_{\Phi} \vec{e}_{jk}^H \rangle \vec{e}_{ik} \diamond_{\Phi} \vec{e}_{kt} \diamond_{\Phi} \vec{e}_{jk}^H,$$



where  $T$  is given as (9). Similarly,

$$\rho^{-1}\mathcal{P}_T\mathcal{P}_\Omega\mathcal{P}_T(\mathcal{Z}) = \sum_{i,j,k} \rho^{-1}\delta_{ijk} \langle \mathcal{Z}, \mathcal{P}_T(\vec{e}_{ik} \diamond_{\Phi} \dot{e}_{kt} \diamond_{\Phi} \vec{e}_{jk}^H) \rangle \mathcal{P}_T(\vec{e}_{ik} \diamond_{\Phi} \dot{e}_{kt} \diamond_{\Phi} \vec{e}_{jk}^H).$$

Define the operator  $\mathcal{T}_{ijk}$  as:

$$\mathcal{T}_{ijk}(\mathcal{Z}) = \rho^{-1}\delta_{ijk} \langle \mathcal{Z}, \mathcal{P}_T(\vec{e}_{ik} \diamond_{\Phi} \dot{e}_{kt} \diamond_{\Phi} \vec{e}_{jk}^H) \rangle \mathcal{P}_T(\vec{e}_{ik} \diamond_{\Phi} \dot{e}_{kt} \diamond_{\Phi} \vec{e}_{jk}^H).$$

Then by the definition of tensor operator norm, we can get

$$\|\mathcal{T}_{ijk}\|_{\text{op}} = \frac{1}{\rho} \|\mathcal{P}_T(\vec{e}_{ik} \diamond_{\Phi} \dot{e}_{kt} \diamond_{\Phi} \vec{e}_{jk}^H)\|_F^2, \text{ and } \|\mathcal{P}_T\|_{\text{op}} \leq 1.$$

Note the fact that  $\mathbf{A}$  and  $\mathbf{B}$  are positive semidefinite matrices, then  $\|\mathbf{A}-\mathbf{B}\| \leq \max\{\|\mathbf{A}\|, \|\mathbf{B}\|\}$ , and combine the inequality given in Proposition 3.2, we have

$$\left\| \mathcal{T}_{ijk} - \frac{1}{n_1 n_2 n_3} \mathcal{P}_T \right\|_{\text{op}} \leq \max \left\{ \frac{1}{\rho} \|\mathcal{P}_T(\vec{e}_{ik} \diamond_{\Phi} \dot{e}_{kt} \diamond_{\Phi} \vec{e}_{jk}^H)\|_F^2, \frac{1}{n_1 n_2 n_3} \right\} \leq \frac{2\mu \sum r_i}{n_{(2)} n_3 \rho}.$$

In addition,

$$\begin{aligned} & \left\| \mathbb{E} \left( \mathcal{T}_{ijk} - \frac{1}{n_1 n_2 n_3} \mathcal{P}_T \right) \right\|_{\text{op}} \\ & \leq \left\| \mathbb{E} \left( \frac{1}{\rho} \|\mathcal{P}_T(\vec{e}_{ik} \diamond_{\Phi} \dot{e}_{kt} \diamond_{\Phi} \vec{e}_{jk}^H)\|_F^2 \mathcal{T}_{ijk} \right) - \frac{2}{n_1 n_2 n_3} \mathcal{P}_T \mathbb{E}(\mathcal{T}_{ijk}) + \frac{1}{n_1^2 n_2^2 n_3^2} \mathcal{P}_T \right\| \\ & = \left\| \frac{1}{\rho} \|\mathcal{P}_T(\vec{e}_{ik} \diamond_{\Phi} \dot{e}_{kt} \diamond_{\Phi} \vec{e}_{jk}^H)\|_F^2 \frac{1}{n_1 n_2 n_3} \mathcal{P}_T - \frac{1}{n_1^2 n_2^2 n_3^2} \mathcal{P}_T \right\| \leq \frac{2\mu \sum r_i}{n_{(1)} n_{(2)}^2 n_3^2 \rho}. \end{aligned}$$

Setting  $\tau = \sqrt{\frac{14\mu\beta \sum r_i \log(n_{(1)} n_3)}{3n_2 n_3 \rho}} \leq \epsilon$  and using Lemma 6.1, we have

$$\begin{aligned} & \mathbb{P}[\|\rho^{-1}\mathcal{P}_T\mathcal{P}_\Omega\mathcal{P}_T - \mathcal{P}_T\|_{\text{op}} > \tau] = \mathbb{P}\left[\left\| \sum_{i,j,k} \left( \mathcal{T}_{ijk} - \frac{1}{n_1 n_2 n_3} \mathcal{P}_T \right) \right\|_{\text{op}} > \tau\right] \\ & \leq 2n_{(1)} n_3 \exp \left( \frac{\frac{14\mu\beta \sum r_i \log(n_{(1)} n_3)}{3n_2 n_3 \rho}}{\frac{2\mu \sum r_i}{n_{(2)} n_3 \rho} + \frac{2\mu \sum r_i}{6n_{(2)} n_3 \rho}} \right) = 2n_{(1)} n_3 \exp(-\beta \log n_{(1)} n_3) = 2n_{(1)} n_3^{1-\beta}, \end{aligned}$$

which implies that

$$\mathbb{P}[\|\rho^{-1}\mathcal{P}_T\mathcal{P}_\Omega\mathcal{P}_T - \mathcal{P}_T\|_{\text{op}} \leq \epsilon] \geq 1 - 2n_{(1)} n_3^{1-\beta}.$$

This completes the proof.

## 6.2 Proof of Lemma 3.4

Denote

$$\rho^{-1}\mathcal{P}_\Omega(\mathcal{Z}) - \mathcal{Z} = \sum_{ijk} \mathcal{T}_{ijk} = \sum_{ijk} \left( \frac{1}{\rho} \delta_{ijk} - 1 \right) \mathcal{Z}_{ijk} \vec{e}_{ik} \diamond_{\Phi} \dot{e}_{kt} \diamond_{\Phi} \vec{e}_{jk}^H.$$

Then by the independence of  $\delta_{ijk}$ , we have  $\mathbb{E}[\mathcal{T}_{ijk}] = 0$  and  $\|\mathcal{T}_{ijk}\| \leq \frac{1}{\rho}\|\mathcal{Z}\|_\infty$ . Moreover,

$$\left\| \mathbb{E} \left[ \sum_{ijk} \mathcal{T}_{ijk}^H \mathcal{T}_{ijk} \right] \right\| = \left\| \sum_{ijk} \mathcal{Z}_{ijk}^2 \vec{e}_{jk} \diamond_{\Phi} \vec{e}_{jk}^H \mathbb{E} \left( \frac{1}{\rho} \delta_{ijk} - 1 \right)^2 \right\| = \left\| \frac{1-\rho}{\rho} \sum_{ijk} \mathcal{Z}_{ijk}^2 \vec{e}_{ik} \diamond_{\Phi} \vec{e}_{ik}^H \right\|.$$

Recall the definition of tensor basis, we can get that  $\Phi(\vec{e}_{jk} \diamond_{\Phi} \vec{e}_{jk}^H)$  is a tensor except the  $(j, j, t)$ -th tube entries equaling  $\Phi(\vec{e}_k)_t^2 = \alpha_t^2, t = 1, \dots, n_3$  with  $\sum_{t=1}^{n_3} \alpha_t^2 = 1$ , and 0 otherwise. It follows that

$$\begin{aligned} \left\| \mathbb{E} \left[ \sum_{ijk} \mathcal{T}_{ijk}^H \mathcal{T}_{ijk} \right] \right\| &= \frac{1-\rho}{\rho} \left\| \sum_{ijk} \mathcal{Z}_{ijk}^2 \vec{e}_{jk} \diamond_{\Phi} \vec{e}_{jk}^H \right\| = \frac{1-\rho}{\rho} \max_j \left\| \sum_{ijk} \mathcal{Z}_{ijk}^2 \vec{e}_{jk} \diamond_{\Phi} \vec{e}_{jk}^H \right\| \\ &= \frac{1-\rho}{\rho} \max_j \left\| \sum_{ik} \mathcal{Z}_{ijk}^2 \vec{e}_{jk} \cdot \vec{e}_{jk}^H \right\| \leq \frac{1}{\rho} \|\mathcal{Z}\|_{\infty, w}^2. \end{aligned}$$

$\left\| \mathbb{E}[\Sigma_{ijk} \mathcal{T}_{ijk} \mathcal{T}_{ijk}^H] \right\|$  can also be bounded. Then by Lemma 6.1, we can get that

$$\|\rho^{-1} \mathcal{P}_\Omega(\mathcal{Z}) - \mathcal{Z}\|_{op} \leq c \left( \frac{\log n_{(1)} n_3}{\rho} \|\mathcal{Z}\|_\infty + \sqrt{\frac{\log n_{(1)} n_3}{\rho}} \|\mathcal{Z}\|_{\infty, w} \right)$$

holds with high probability provided that  $m \geq C_0 \epsilon^{-2} \mu \sum r_i n_{(1)} \log(n_{(1)} n_3)$ .

### 6.3 Proof of Lemma 3.5

Denote the weighted  $b$ -th tensor column of  $(\rho^{-1} \mathcal{P}_T \mathcal{P}_\Omega - \mathcal{P}_T) \mathcal{Z}$  as

$$\sum_{ijk} \mathcal{T}_{ijk} := (\rho^{-1} \mathcal{P}_T \mathcal{P}_\Omega - \mathcal{P}_T) \mathcal{Z} \diamond_{\Phi} \vec{e}_{bk} = \sum_{ijk} \left( \frac{1}{\rho} \delta_{ijk} - 1 \right) \mathcal{Z}_{ijk} P_T(\vec{e}_{ik} \diamond_{\Phi} \vec{e}_{kt} \diamond_{\Phi} \vec{e}_{jk}^H) \diamond_{\Phi} \vec{e}_{bk},$$

where  $\mathcal{T}_{ijk}$  are zero-mean independent tensor columns. By the incoherence conditions given in Proposition 3.2, we have

$$\|\mathcal{T}_{ijk}\|_F = \left\| \left( \frac{1}{\rho} \delta_{ijk} - 1 \right) \mathcal{Z}_{ijk} P_T(\vec{e}_{ik} \diamond_{\Phi} \vec{e}_{kt} \diamond_{\Phi} \vec{e}_{jk}^H) \diamond_{\Phi} \vec{e}_{bk} \right\|_F \leq \frac{1}{\rho} \sqrt{\frac{2\mu r}{n}} \|\mathcal{Z}\|_\infty.$$

Furthermore,

$$\left| \mathbb{E} \left[ \sum_{ijk} \mathcal{T}_{ijk}^H \diamond_{\Phi} \mathcal{T}_{ijk} \right] \right| = \frac{1-\rho}{\rho} \sum_{i,j,k} \mathcal{Z}_{ijk}^2 \|P_T(\vec{e}_{ik} \diamond_{\Phi} \vec{e}_{kt} \diamond_{\Phi} \vec{e}_{jk}^H) \diamond_{\Phi} \vec{e}_{bk}\|_F^2.$$

Then by the definition of  $\mathcal{P}_T$ , we can get

$$\begin{aligned} &\|P_T(\vec{e}_{ik} \diamond_{\Phi} \vec{e}_{kt} \diamond_{\Phi} \vec{e}_{jk}^H) \diamond_{\Phi} \vec{e}_{bk}\|_F^2 \\ &= \|\mathcal{U} \diamond_{\Phi} \mathcal{U}^H \diamond_{\Phi} \vec{e}_{ik} \diamond_{\Phi} \vec{e}_{kt} \diamond_{\Phi} \vec{e}_{jk}^H \diamond_{\Phi} \vec{e}_{bk} + (\mathcal{I} - \mathcal{U} \diamond_{\Phi} \mathcal{U}^H) \diamond_{\Phi} \vec{e}_{ik} \diamond_{\Phi} \vec{e}_{kt} \diamond_{\Phi} \vec{e}_{jk}^H \diamond_{\Phi} \mathcal{V} \diamond_{\Phi} \mathcal{V}^H \diamond_{\Phi} \vec{e}_{bk}\|_F^2 \\ &\leq \frac{\mu r}{n} \|\vec{e}_{kt} \diamond_{\Phi} \vec{e}_{jk} \diamond_{\Phi} \vec{e}_{bk}\|_F^2 + \|\vec{e}_{jk}^H \diamond_{\Phi} \mathcal{V} \diamond_{\Phi} \mathcal{V}^H \diamond_{\Phi} \vec{e}_{bk}\|_F^2. \end{aligned}$$

Therefore,

$$\begin{aligned}
\left| \mathbb{E} \left[ \sum_{ijk} \mathcal{T}_{ijk}^H \diamond_{\Phi} \mathcal{T}_{ijk} \right] \right| &\leq \frac{2}{\rho} \sum_{i,j,k} \mathcal{Z}_{ijk}^2 \|P_T(\vec{e}_{ik} \diamond_{\Phi} \vec{e}_{kt} \diamond_{\Phi} \vec{e}_{jk}^H) \diamond_{\Phi} \vec{e}_{bk}\|_{\text{F}}^2 \\
&\leq \frac{2}{\rho} \sum_{i,j,k} \mathcal{Z}_{ijk}^2 \frac{\mu r}{n} \|\vec{e}_{kt} \diamond_{\Phi} \vec{e}_{jk} \diamond_{\Phi} \vec{e}_{bk}\|_{\text{F}}^2 + \frac{2}{\rho} \sum_{i,j,k} \mathcal{Z}_{ijk}^2 \|\vec{e}_{jk}^H \diamond_{\Phi} \mathcal{V} \diamond_{\Phi} \mathcal{V}^H \diamond_{\Phi} \vec{e}_{bk}\|_{\text{F}}^2 \\
&\leq \frac{2\mu r}{\rho n} \|\mathcal{Z}\|_{\infty, w}^2 + \frac{2}{\rho} \sum_{i,j,k} \mathcal{Z}_{ijk}^2 \|\vec{e}_{jk}^H \diamond_{\Phi} \mathcal{V} \diamond_{\Phi} \mathcal{V}^H \diamond_{\Phi} \vec{e}_{jk}\|_{\text{F}}^2 \\
&\leq \frac{4\mu r}{n} \|\mathcal{Z}\|_{\infty, w}^2,
\end{aligned}$$

where the third inequality holds by  $\vec{e}_{jk}^H \diamond_{\Phi} \vec{e}_{bk} = 0$  if  $j \neq b$ . By the same argument,  $\left| \mathbb{E}[\sum_{ijk} \mathcal{T}_{ijk} \diamond_{\Phi} \mathcal{T}_{ijk}^H] \right|$  can be bounded by the same quantity. Therefore, by Lemma 6.1, we get that

$$\|(\rho^{-1} \mathcal{P}_T \mathcal{P}_{\Omega} - \mathcal{P}_T) \mathcal{Z} \diamond_{\Phi} \vec{e}_{bk}\|_{\text{F}} \leq \frac{1}{2} \|\mathcal{Z}\|_{\infty, w} + \frac{1}{2} \sqrt{\frac{n}{\mu r}} \|\mathcal{Z}\|_{\infty}$$

holds with high probability. We can also get the same results relate to  $\vec{e}_{ak}^H \diamond_{\Phi} (\rho^{-1} \mathcal{P}_T \mathcal{P}_{\Omega} - \mathcal{P}_T) \mathcal{Z}$ . Then Lemma 3.5 follows from using a union bound over all the tensor columns and rows, and the results hold with high probability.

## References

- [1] B. Barak and A. Moitra. Noisy tensor completion via the sum-of-squares hierarchy. In *Conference on Learning Theory*, pages 417–445, 2016.
- [2] E. J. Candès, X. Li, Y. Ma, and J. Wright. Robust principal component analysis? *Journal of the ACM*, 58(3):11, 2011.
- [3] E. J. Candès and Y. Plan. Matrix completion with noise. *Proceedings of the IEEE*, 98(6):925–936, 2010.
- [4] E. J. Candès and B. Recht. Exact matrix completion via convex optimization. *Foundations of Computational Mathematics*, 9(6):717–772, 2009.
- [5] E. J. Candès and T. Tao. The power of convex relaxation: Near-optimal matrix completion. *IEEE Transactions on Information Theory*, 56(5):2053–2080, 2010.
- [6] Y. Chen. Incoherence-optimal matrix completion. *IEEE Transactions on Information Theory*, 61(5):2909–2923, 2015.
- [7] M. Fazel, T. K. Pong, D. Sun, and P. Tseng. Hankel matrix rank minimization with applications to system identification and realization. *SIAM Journal on Matrix Analysis and Applications*, 34(3):946–977, 2013.
- [8] R. Glowinski and A. Marroco. Sur l’approximation, par éléments finis d’ordre un, et la résolution, par pénalisation-dualité d’une classe de problèmes de Dirichlet non linéaires. *Revue Française d’Automatique Informatique, Recherche Opérationnelle. Analyse Numérique*, 9(R2):41–76, 1975.

- [9] D. Gross. Recovering low-rank matrices from few coefficients in any basis. *IEEE Transactions on Information Theory*, 57(3):1548–1566, 2011.
- [10] B. Huang, C. Mu, D. Goldfarb, and J. Wright. Provable models for robust low-rank tensor completion. *Pacific Journal of Optimization*, 11(2):339–364, 2015.
- [11] T. Imbiriba, R. A. Borsoi, and J. C. M. Bermudez. A low-rank tensor regularization strategy for hyperspectral unmixing. In *2018 IEEE Statistical Signal Processing Workshop (SSP)*, pages 373–377. IEEE, 2018.
- [12] P. Jain and S. Oh. Provable tensor factorization with missing data. In *Advances in Neural Information Processing Systems*, pages 1431–1439, 2014.
- [13] E. Kernfeld, M. Kilmer, and S. Aeron. Tensor-tensor products with invertible linear transforms. *Linear Algebra and its Applications*, 485:545–570, 2015.
- [14] M. E. Kilmer, K. Braman, N. Hao, and R. C. Hoover. Third-order tensors as operators on matrices: A theoretical and computational framework with applications in imaging. *SIAM Journal on Matrix Analysis and Applications*, 34(1):148–172, 2013.
- [15] M. E. Kilmer and C. D. Martin. Factorization strategies for third-order tensors. *Linear Algebra and its Applications*, 435(3):641–658, 2011.
- [16] T. G. Kolda and B. W. Bader. Tensor decompositions and applications. *SIAM Review*, 51(3):455–500, 2009.
- [17] A. Krishnamurthy and A. Singh. Low-rank matrix and tensor completion via adaptive sampling. In *Advances in Neural Information Processing Systems*, pages 836–844, 2013.
- [18] J. Liu, P. Musialski, P. Wonka, and J. Ye. Tensor completion for estimating missing values in visual data. *IEEE Transactions on Pattern Analysis and Machine Intelligence*, 35(1):208–220, 2013.
- [19] C. D. Martin, R. Shafer, and B. LaRue. An order-p tensor factorization with applications in imaging. *SIAM Journal on Scientific Computing*, 35(1):A474–A490, 2013.
- [20] A. Montanari and N. Sun. Spectral algorithms for tensor completion. *Communications on Pure and Applied Mathematics*, 71(11):2381–2425, 2018.
- [21] C. Mu, B. Huang, J. Wright, and D. Goldfarb. Square deal: Lower bounds and improved relaxations for tensor recovery. In *International Conference on Machine Learning*, pages 73–81, 2014.
- [22] M. K. Ng. *Iterative Methods for Toeplitz Systems*. Oxford University Press, Oxford, 2004.
- [23] M. K. Ng, Q. Yuan, L. Yan, and J. Sun. An adaptive weighted tensor completion method for the recovery of remote sensing images with missing data. *IEEE Transactions on Geoscience and Remote Sensing*, 55(6):3367–3381, 2017.
- [24] B. Recht. A simpler approach to matrix completion. *Journal of Machine Learning Research*, 12:3413–3430, 2011.
- [25] B. Recht, M. Fazel, and P. A. Parrilo. Guaranteed minimum-rank solutions of linear matrix equations via nuclear norm minimization. *SIAM Review*, 52(3):471–501, 2010.

- [26] B. Romera-Paredes, H. Aung, N. Bianchi-Berthouze, and M. Pontil. Multilinear multitask learning. In *International Conference on Machine Learning*, pages 1444–1452, 2013.
- [27] M. Signoretto, Q. T. Dinh, L. De Lathauwer, and J. A. Suykens. Learning with tensors: a framework based on convex optimization and spectral regularization. *Machine Learning*, 94(3):303–351, 2014.
- [28] G.-J. Song, M. K. Ng, and X. Zhang. Robust tensor completion using transformed tensor singular value decomposition. *Numer Linear Algebra Appl.*, 27(3):e2299, 2020.
- [29] R. Tomioka, T. Suzuki, K. Hayashi, and H. Kashima. Statistical performance of convex tensor decomposition. In *Advances in Neural Information Processing Systems*, pages 972–980, 2011.
- [30] L. R. Tucker. Some mathematical notes on three-mode factor analysis. *Psychometrika*, 31(3):279–311, 1966.
- [31] Z. Wang, A. C. Bovik, H. R. Sheikh, and E. P. Simoncelli. Image quality assessment: From error visibility to structural similarity. *IEEE Transactions on Image Processing*, 13(4):600–612, 2004.
- [32] D. Xia and M. Yuan. On polynomial time methods for exact low rank tensor completion. *Foundations of Computational Mathematics*, 2019.
- [33] J.-H. Yang, X.-L. Zhao, T.-H. Ma, Y. Chen, T.-Z. Huang, and M. Ding. Remote sensing images destriping using unidirectional hybrid total variation and nonconvex low-rank regularization. *Journal of Computational and Applied Mathematics*, 363:124–144, 2020.
- [34] M. Yuan and C.-H. Zhang. On tensor completion via nuclear norm minimization. *Foundations of Computational Mathematics*, 16(4):1031–1068, 2016.
- [35] M. Yuan and C.-H. Zhang. Incoherent tensor norms and their applications in higher order tensor completion. *IEEE Transactions on Information Theory*, 63(10):6753–6766, 2017.
- [36] X. Zhang and M. K. Ng. A corrected tensor nuclear norm minimization method for noisy low-rank tensor completion. *SIAM Journal on Imaging Sciences*, 12(2):1231–1273, 2019.
- [37] Z. Zhang and S. Aeron. Exact tensor completion using t-SVD. *IEEE Transactions on Signal Processing*, 65(6):1511–1526, 2017.
- [38] F. Zhu, Y. Wang, B. Fan, S. Xiang, G. Meng, and C. Pan. Spectral unmixing via data-guided sparsity. *IEEE Transactions on Image Processing*, 23(12):5412–5427, 2014.